Monthly Notices
of the
ROYAL ASTRONOMICAL SOCIETY

MNRAS **442,** 2253–2270 (2014) doi:10.1093/mnras/stu962

Herschel-ATLAS/GAMA: How does the far-IR luminosity function depend on galaxy group properties?

Qi Guo,[1,2⋆] Cedric Lacey,[1] Peder Norberg,[1] Shaun Cole,[1] Carlton Baugh,[1] Carlos Frenk,[1] Asantha Cooray,[3] Simon Dye,[4] N. Bourne,[4] L. Dunne,[5] S. Eales,[6] R. J. Ivison,[7] S. J. Maddox,[5] M. Alpasan,[8] I. Baldry,[9] J. Bland-Hawthorn,[10] S. P. Driver[8,11] and A. Robotham[11]

[1]*Institute for Computational Cosmology, Department of Physics, University of Durham, South Road, Durham DH1 3LE, UK*
[2]*Partner Group of the Max-Planck-Institut für Astrophysik, National Astronomical Observatories, Chinese Academy of Sciences, Beijing, 100012, China*
[3]*Department of Physics and Astronomy, University of California, Irvine, CA,92697, USA*
[4]*School of Physics and Astronomy, University of Nottingham, Nottingham NG7 2RD, UK*
[5]*Department of Physics and Astronomy, University of Canterbury, Private Bag 4800, Christchurch, New Zealand*
[6]*School of Physics and Astronomy, Cardiff University, The Parade, Cardiff CF24 3AA, UK*
[7]*UK Astronomy Technology Centre, Royal Observatory, Blackford Hill, Edinburgh EH9 3HJ, UK*
[8]*Scottish Universities Physics Alliance (SUPA), School of Physics and Astronomy, University of St Andrews, North Haugh, St Andrews KY16 9SS, UK*
[9]*Astrophysics Research Institute, Liverpool John Moores University, IC2, Liverpool Science Park, 146 Brownlow Hill, Liverpool, L3 5RF, UK*
[10]*Sydney Institute for Astronomy, University of Sydney, NSW 2006, Australia*
[11]*International Centre for Radio Astronomy Research (ICRAR), University of Western Australia, Crawley, WA 6009, Australia*

Accepted 2014 May 12. Received 2014 April 7; in original form 2014 January 5

ABSTRACT

We use the *Herschel* Astrophysical Terahertz Large Area Survey (H-ATLAS) Phase I data to study the conditional luminosity function of far-IR (250 μm) selected galaxies in optically selected galaxy groups from the Galaxy And Mass Assembly (GAMA) spectroscopic survey, as well as environmental effects on the far-IR-to-optical colour. We applied two methods, which gave consistent results for the far-IR conditional luminosity functions. The direct matching method matches H-ATLAS sources to GAMA/SDSS (Sloan Digital Sky Survey) galaxies, then links the optical counterparts to GAMA groups. The stacking method counts the number of far-IR sources within the projected radii of GAMA groups, subtracting the local background. We investigated the dependence of the far-IR (250 μm) luminosity function on group mass in the range $10^{12} < M_{\rm h} < 10^{14}\,h^{-1}\,{\rm M}_{\odot}$ and on redshift in the range $0 < z < 0.4$, using a sample of 3000 groups containing H-ATLAS sources with GAMA redshifts over an area of 126 deg^2. We find that the characteristic 250 μm luminosity, $L^*(250)$, increases with group mass up to $M_{\rm h} \sim 10^{13}\,h^{-1}\,{\rm M}_{\odot}$, but is roughly constant above this, while it increases with redshift at high group masses, but less so at low masses. We also find that the group far-IR luminosity-to-mass ratio $L(250)/M_{\rm h}$ increases with redshift and is higher in low-mass groups. We estimate that around 70 per cent of the 250 μm luminosity density in the local Universe is contributed by groups with $M_{\rm h} > 10^{12}\,h^{-1}\,{\rm M}_{\odot}$. We also find that the far-IR-to-optical colours of H-ATLAS galaxies are independent of group mass over the range $10^{12} < M_{\rm h} < 10^{14}\,h^{-1}\,{\rm M}_{\odot}$ in the local Universe. We also compare our observational results with recent semi-analytical models, and find that none of these galaxy formation models can reproduce the conditional far-IR luminosity functions of galaxy groups.

Key words: galaxies: clusters: general – galaxies: formation – galaxies: haloes – galaxies: luminosity function, mass function – cosmology: theory – infrared: galaxies.

1 INTRODUCTION

Star formation is one of the most important processes determining the formation and evolution of the galaxies. Theoretical work

⋆ E-mail: qi.guo2010@gmail.com

suggests that in situ star formation dominates over the accretion and mergers of satellite galaxies for the growth in stellar mass of galaxies less massive than the Milky Way at all redshifts (e.g. Guo & White 2008; Parry, Eke & Frenk 2009). Even at the Milky Way mass, star formation is the primary means of adding stellar mass at $z \gtrsim 1$. Observational studies have measured star formation rates (SFRs) from the local Universe to high redshifts. A picture in which the overall star formation density increases with redshift and peaks at around $z \sim 2$ has now been well established (e.g. Madau, della Valle & Panagia 1998; Hopkins 2007). Methods to infer the SFR include the direct measurement of the rest-frame UV luminosity (e.g. Lilly et al. 1996; Madau et al. 1998; Steidel et al. 1999; Salim et al. 2007), or emission lines such as Hα and [O II] emission lines (e.g. Gallego et al. 1995; Brinchmann et al. 2004; Sobral et al. 2011), all of which trace massive young stars. However, these methods are subject to uncertain corrections for dust extinction, which varies in the regions of different local properties, as well as depending on the inclination of the galaxy. UV photons heat the dust around star-forming regions and are then reprocessed by the dust and their energy is re-emitted in the mid- and far-IR range, with the dust emission typically peaking at a wavelength around 100μm. About half of the starlight is absorbed and re-emitted over the history of the Universe (Puget et al. 1996; Hauser et al. 1998) (some studies show that an even larger fraction of the UV light is reprocessed, e.g. Buat et al. 2007). Observations at IR wavelengths are thus an essential complement to UV and optical tracers of star formation. Previous surveys in the IR include that by *IRAS*, which measured the far-IR emission at ≤100 μm, which mainly constrains the emission from warm dust in bright galaxies (Dunne & Eales 2001), while more recent surveys of dust emission focused either on the mid-IR (*ISO*, *Spitzer*) or sub-mm (e.g. Submillimetre Common-User Bolometer Array) wavelengths, and therefore misses the peak in the dust emission, and hence requires uncertain extrapolations to infer total IR luminosities. *Herschel* [1] (Pilbratt et al. 2010) observations span the far-IR wavelengths 60–700 μm, covering the peak of the dust emission from star-forming galaxies. Moreover, as the largest open-time key project on *Herschel*, the *Herschel* Astrophysical Terahertz Large Area Survey (H-ATLAS; Eales et al. 2010a) provides far-IR imaging and photometry over an area of 550 deg^2, in five channels centred on 100, 160, 250, 350, and 500 μm, ideal for using the far-IR emission to estimate the dust obscured SFR.

The SFR of galaxies depends on stellar mass, redshift, and environment. It has been known for many years that the fraction of star-forming galaxies decreases as the mass of the host dark matter halo increases, from isolated field galaxies up to rich clusters (e.g. Dressler 1980; Kimm et al. 2009). The fraction of actively star-forming galaxies in groups and clusters also increases with redshift (e.g. Butcher & Oemler 1978). However, focusing only on the population of star-forming galaxies, the effect of galaxy environment on star formation activity is still under debate. Most studies find no dependence of the SFR of star-forming galaxies at a given stellar mass on group/cluster environment or local density, from low ($z = 0$) to intermediate ($z < 0.5$) redshifts (Balogh et al. 2004; Tanaka et al. 2004; Weinmann et al. 2006; Peng et al. 2010; McGee et al. 2011). This independence has also been found at high redshift ($z \sim 1$) (Ideue et al. 2012). However, some other studies conflict with this conclusion (Lewis et al. 2002; Gómez et al. 2003; Welikala et al. 2008), suggesting that galaxy SFRs are more strongly suppressed in highly overdense regions.

Most previous work on the dependence of galactic SFRs on environment has used the UV continuum or the Hα emission to estimate SFRs. In this paper, we revisit this problem by looking at an important tracer of the dust-obscured SFR, the far-IR emission. Early work on the IR properties of galaxies in rich clusters based on *IRAS* and *Infrared Space Observatory* (*ISO*) observations is reviewed by Metcalfe, Fadda & Biviano (2005). There have been several studies using mid-IR observations, mainly the *Spitzer* 24 μm band, to estimate the IR luminosity functions (LFs) of galaxy clusters ($M \gtrsim 10^{14}\,\mathrm{M}_\odot$) (e.g Bai et al. 2006, 2009; Chung et al. 2010; Finn et al. 2010; Goto et al. 2010; Biviano et al. 2011), and one measurement of the IR LF of massive galaxy groups ($10^{13} \lesssim M \lesssim 10^{14}\,\mathrm{M}_\odot$) (Tran et al. 2009). However, these studies had the drawback that they had to extrapolate in wavelength in order to estimate total IR luminosities. SFRs estimated from mid-IR luminosities have been used to study the fraction of star-forming galaxies in different density environments (e.g. Koyama et al. 2008; Tran et al. 2009), and also to study the dependence of the specific star formation rate (sSFR), defined as the ratio, SFR/$M_\star$, of SFR to stellar mass M_*, on local density and group or cluster environment (e.g. Elbaz et al. 2007; Bai et al. 2010). Mid-IR observations have also been used to estimate the evolution of the ratio $L_{\rm IR}/M_{\rm h}$ of total IR luminosity to dark matter halo mass $M_{\rm h}$ for rich clusters (Geach et al. 2006; Koyama et al. 2010; Webb et al. 2013). These studies have recently been extended to the far-IR and to galaxy groups by Popesso et al. (2012), who used *Herschel* observations to measure $L_{\rm IR}/M_{\rm h}$ for 9 rich clusters ($M \sim 10^{15}\,\mathrm{M}_\odot$) and nine groups ($M \sim 5 \times 10^{13}\,\mathrm{M}_\odot$) at redshifts $0.1 \lesssim z \lesssim 1$.

In this paper, we directly measure the far-IR LFs and $L_{\rm IR}/M_{\rm h}$ ratios of a very large sample (∼3000) of galaxy groups and clusters covering a wide range in mass, $10^{12} < M_{\rm h} < 10^{14}\,h^{-1}\,\mathrm{M}_\odot$, in the low-redshift $z < 0.4$ Universe using data from *Herschel*. We also use our sample to measure the dependence of the dust-obscured sSFR on group mass. The galaxy groups are optically selected from the Galaxy And Mass Assembly (GAMA) spectroscopic survey (Driver et al. 2009). Our study has several advantages over previous studies of the same range of group mass and redshift: (a) we use far-IR observations, which provide a much more robust measure of the total IR luminosity, and hence of the dust-obscured SFR, than is possible using mid-IR data; (b) we probe a much larger range of group mass than was available to previous studies, which were restricted to quite massive groups, $10^{13} \lesssim M_{\rm h} \lesssim 10^{14}\,h^{-1}\,\mathrm{M}_\odot$; (c) we have a much larger sample of groups than previous studies, which had samples of ∼10 groups at most. (d) our group sample, being optically selected, is much more complete than the X-ray selected samples used in many previous IR studies. (e) We study the IR LF of groups down to $L_{\rm IR} \sim 10^9\,\mathrm{L}_\odot$, much fainter than most previous studies of groups and clusters, which were restricted to $L_{\rm IR} \sim 10^{10}\,\mathrm{L}_\odot$ or brighter.

The first step in our study is to measure the galaxy abundance in groups and clusters as a function of their far-IR luminosities. Similar techniques have been developed extensively in the optical range (e.g. Jing, Mo & Boerner 1998; Berlind & Weinberg 2002; Yang, Mo & van den Bosch 2003), while the far-IR is almost unexplored due to the previous lack of deep and sufficiently large surveys at these wavelengths. The H-ATLAS is a perfect survey for this study. To identify galaxy groups, we use group catalogues (Robotham et al. 2011) based on an optical redshift survey – the GAMA I survey (Baldry et al. 2010; Driver et al. 2009, 2011; Hill et al. 2011; Taylor et al. 2011; Kelvin et al. 2012). The abundance

[1] *Herschel* is an ESA (European Space Agency) space observatory with science instruments provided by European-led Principal Investigator consortia and with important participation from NASA.

of far-IR galaxies within a given GAMA group is then measured using two methods. One is to match H-ATLAS sources to GAMA galaxies (Smith et al. 2011), calculating the abundance of the far-IR-detected group members directly. The other is to calculate the abundance of H-ATLAS sources within a projected radius around the group centre after subtracting the contribution from the background. After measuring the far-IR conditional luminosity function (CLF) for groups of different masses and redshifts, we further study its properties, including the characteristic far-IR luminosity L^* and luminosity-to-mass ratio, and their correlation with the masses and redshifts of the host groups. The first method also enables us to study the variation of the far-IR-to-optical colour (which is an indicator of the sSFR) in the field, groups, and clusters.

This paper is organized as follows. In Section 2, we briefly describe the two catalogues used in this work: H-ATLAS Phase I and GAMA-I (including groups). The two methods used to count group members, as well as the data description are also presented in Section 2. The far-IR LFs in groups of different masses and redshifts are presented in Section 3. In this section, we also discuss the relationship between the total far-IR luminosity and group mass and its evolution with redshift. In Section 4, we discuss the far-IR-to-optical colour, focusing on environmental effects and redshift evolution. A comparison with predictions from galaxy formation models is presented in Section 5. Our main results are summarized in Section 6.

Throughout this paper, we assume a flat Λ cold dark matter (ΛCDM) cosmology with $\Omega_{\rm m} = 0.25$, $\Omega_\Lambda = 0.75$, h $= 0.73$, where $H_0 = 100\,{\rm km\,s^{-1}\,Mpc^{-1}}$ and power spectrum normalization $\sigma_8 = 0.9$. This power spectrum normalization is only relevant for our model predictions as presented in Section 5.

2 DATA AND METHODS

In Section 2.1, we describe the GAMA data; in Section 2.2, the H-Atlas data, and in Section 2.3, we outline how we measure the luminosity of groups.

2.1 GAMA-I

The GAMA-I survey is an optical spectroscopic galaxy survey covering 142 deg^2 in three equal-sized regions on the celestial equator, to apparent r-band magnitude $r_{AB} = 19.4$ in two regions (G09 and G15) and $r_{AB} = 19.8$ in one region (G12).[2] It contains 110 192 galaxies with optical/near-IR imaging [from the Sloan Digital Sky Survey (SDSS), the UKIRT(United Kingdom Infrared Telescope) Infrared Deep Sky Survey, the Kilo-Degree Survey, VISTA (the Visible and Infrared Survey Telescope for Astronomy) Kilo-Degree Infrared Galaxy Survey, with the latter two still underway], and complementary observations from the UV [the Galaxy Evolution Explorer (GALEX)] through to the mid- and far-IR [*Wide-field Infrared Survey Explorer (WISE), Herschel*] and the radio [*Australian Square Kilometre Array Pathfinder (ASKAP), Giant Metrewave Radio Telescope (GMRT)*, underway]. The redshift completeness to r-band magnitude 19.4 reaches 98.7 per cent (Driver et al. 2011). To simplify the selection function, we limit ourselves to $r < 19.4$. This leads to a sample of 93 325 galaxies, with a redshift coverage of $0 < z < 0.5$ centred at around $z \sim 0.2$.

[2] The GAMA-II survey reaches $r_{AB} = 19.8$ in all fields. However, the group catalogue we use is based on GAMA-I. In order to have a self-consistent analysis, we adopt the GAMA-I data release rather than the GAMA-II survey.

Using the GAMA-I optically selected redshift catalogue, Robotham et al. (2011) used a redshift space friends-of-friends grouping algorithm to create the GAMA-I group catalogue. Systems with two or more optical members are identified as galaxy groups. In total, there are 12.2k GAMA groups, and around 34 per cent of GAMA galaxies belong to groups. Total group masses used in this study are inferred from the total r-band luminosity of the group, its redshift and the group multiplicity, following the description given in Robotham et al. (2011) and implemented in Han et al. (2014). The GAMA group catalogue has been extensively tested against a set of mock GAMA lightcones, following the method described in Merson et al. (2013). In summary, the mocks are constructed from the Millennium ΛCDM dark matter N-body simulation (Springel et al. 2005), populated with galaxies using the GALFORM semi-analytical galaxy formation model (Cole et al. 2000), using the Bower et al. (2006) model as input. Finally, the raw GALFORM lightcones are abundance matched to precisely reproduce the GAMA r-band LF (Loveday et al. 2012), resulting in minor modifications to the r-band magnitudes (typically less than 0.1 mag). This is consistent with differences expected to arise from different magnitude definitions, which are not included in the lightcone pipeline. Readers are referred to Merson et al. (2013) and Robotham et al. (2011) for further details on the mocks, and in particular to the latter for a list of known limitations specific to the GAMA lightcone mocks.

For the present study, the completeness of the group catalogue as function of group mass and redshift needs to be addressed. Using the mocks, we estimate this completeness to be about 90 per cent for $z < 0.2$ and $M_h > 10^{13}\,{\rm M}_\odot\,h^{-1}$, while it decreases strongly with decreasing group mass and increasing redshift to below 20 per cent, for e.g. groups less massive than $10^{13}\,{\rm M}_\odot\,h^{-1}$ in the redshift range $0.1<z<0.3$. These completenesses correspond to upper limits, as they do not account for uncertainties in the group mass estimate, nor in the grouping. A comprehensive investigation, including uncertainties from applying the group finder to a different set of mocks, is currently underway and beyond the scope of this paper. We note here that the underlying assumption for the rest of the paper is that the identified groups of a given mass are an unbiased sample of all groups of that mass.

2.2 H-ATLAS Phase I

The H-ATLAS Phase I Data Release consists of three equatorial fields (G09, G12, and G15), covering 135 deg^2 in total. The overlap between H-ATLAS and the GAMA-I survey is about 126 deg^2. H-ATLAS has imaging in five far-IR bands centred on 100, 160, 250, 350, and 500 μm, using the Photodetector Array Camera and Spectrometer (PACS) (Poglitsch et al. 2010) and the Spectral and Photometric Imaging Receiver (SPIRE) (Griffin et al. 2010) instruments. The median values of the 5σ flux limits are 132, 126, 32, 36, and 45 mJy, respectively, for the five wavelengths. There are 78.0 k sources brighter than the 5σ detection limit in one or more of the three SPIRE bands (Rigby et al. 2011). In this paper, we work with a 250 μm flux-limited sample, since this is the most sensitive band and has the best positional accuracy of the three SPIRE bands.

In the H-ATLAS Phase I Data Release, sources brighter than the 5σ flux limit at 250 μm have been matched to the r-band selected ($r < 22.4$) SDSS galaxy imaging catalogue using a likelihood ratio method (Sutherland & Saunders 1992). The application of the method to the H-ATLAS survey is described in detail in Smith et al. (2011), but we give a brief description here. For a potential optical counterpart with r-band apparent magnitude m at angular distance r from the estimated position of the H-ATLAS source, the likelihood ratio L is calculated as $L = \frac{q(m)f(r)}{n(m)}$, and gives the ratio of the

probability that the optical source is the correct ID to the corresponding probability that it is an unrelated background source. The positional errors for the H-ATLASsources, which determine the radial probability distribution *f(r)*, are determined using histograms of the separations between the positions of 250 μm sources and those of galaxies in the SDSS DR7 *r*-band catalogue within 50 arcsec. *n(m)* is the probability that a background SDSS source is observed with magnitude *m*, which is well defined. *q(m)* is the probability for a true counterpart to a 250 μm source to have a magnitude *m*, which is calculated as the normalized magnitude distribution of the SDSS sources within 10 arcsec of each 250 μm source after subtracting the background, multiplied by the fraction Q_0 of true counterparts which are above the SDSS limit. Smith et al. (2011) measure $Q_0 = 0.59$. A reliability value ($R_{\rm LR}$) is then assigned to each potential optical counterpart (hereafter candidate), which allows for the presence of other optical candidates. $R_{\rm LR}$ is the Bayesian probability that the candidate is the true counterpart. Following Smith et al., we take the threshold for a reliable match as $R_{\rm LR} > 0.8$, for which choice they estimate that 96 per cent of the assigned IDs are the true optical counterparts.

For this paper, we use the sample of 66.2 k H-ATLASsources with 250 μm flux above 35 mJy, which is higher than the median 5σ value to guarantee a uniform selection. There are then 29.8 k candidate optical counterparts with $R_{\rm LR} > 0.8$ (45 per cent of our total 250 μm H-ATLASsample). Out of this matched sample, 24.2 k galaxies are in the area overlapping with the GAMA-I survey. Applying a uniform cut of $r < 19.4$ in all three regions overlapping with GAMA-I leads to 10.5 k H-ATLASgalaxies with reliable counterparts in the GAMA spectroscopic sample, corresponding to 43 per cent of the sources with an optical counterpart in SDSS in the GAMA-I overlap region. This sample with spectroscopic redshifts forms the direct matching catalogue which we use in most of this work.

In this paper, we study H-ATLAS galaxies at $z < 0.4$. An important question is whether a significant fraction of such galaxies have optical counterparts which are too faint to appear in the SDSS imaging catalogue. To answer this question, we use data from the Herschel Multi-tiered Extragalactic Survey (HerMES; Oliver 2012) of the Cosmic Evolution Survey (COSMOS) field, which also has very deep optical, 3.6 μm and 24 μm imaging data. The HerMES team find optical counterparts to *Herschel* sources by first matching *Herschel* sources to 24 μm sources (Roseboom et al. 2010, 2012), which method is estimated to be highly complete for this field at the fluxes of interest here ($S(250\,\mu{\rm m}) > 35$ mJy). The 24 μm sources are then matched to the closest 3.6 μm source within 2 arcsec, and each 3.6 μm source is matched to the nearest optical source within 1 arcsec. They then obtain redshifts for these sources from the COSMOS photometric redshift catalogue (Ilbert et al. 2009). In this way, they measure a highly complete redshift distribution for *Herschel* sources with $S(250\,\mu{\rm m}) > 35$ mJy. From this catalogue, they find that all sources with $S(250\,\mu{\rm m}) > 35$ mJy and having optical counterparts fainter than $r > 22.4$ lie at redshifts $z > 0.4$ (Lingyu Wang, private communication).

There are 10.7 k GAMA groups in the H-ATLAS overlap region, of which 3.0 k groups have mass $10^{12} < M_{\rm h} < 10^{14}\,h^{-1}\,{\rm M}_\odot$ and redshifts in the range $0 < z < 0.4$ and contain 1 or more reliable $r < 19.4$ counterparts in H-ATLAS. In total there are 3.2 k H-ATLAS-GAMA galaxies in GAMA groups.

Note that the full width at half-maximum beamsize of *Herschel* is about 18 arcsec at 250 μm, which could potentially lead to source confusion, especially in high-density regions like groups. The general effects of confusion in the H-ATLAS survey were found by Rigby et al. (2011) to be modest at 250 μm. In Fig. 1, we show the size distribution of the GAMA groups in different ranges of redshift and mass, compared to the beamsize of *Herschel* at 250 μm. Since the group size is an increasing function of group mass, at each redshift we only present the lowest group mass range which contains H-ATLAS galaxies. The figure shows that only a few per cent of the groups in our sample have angular sizes comparable to or smaller than the beam radius of *Herschel* at 250 μm. We have also visually checked the spatial distribution of GAMA galaxies in a random subset of groups, and find that in most cases, the separations between optical members are much larger than the beamsize at 250μm. We therefore conclude that the effects of source confusion due to other group members should be very small for this study.

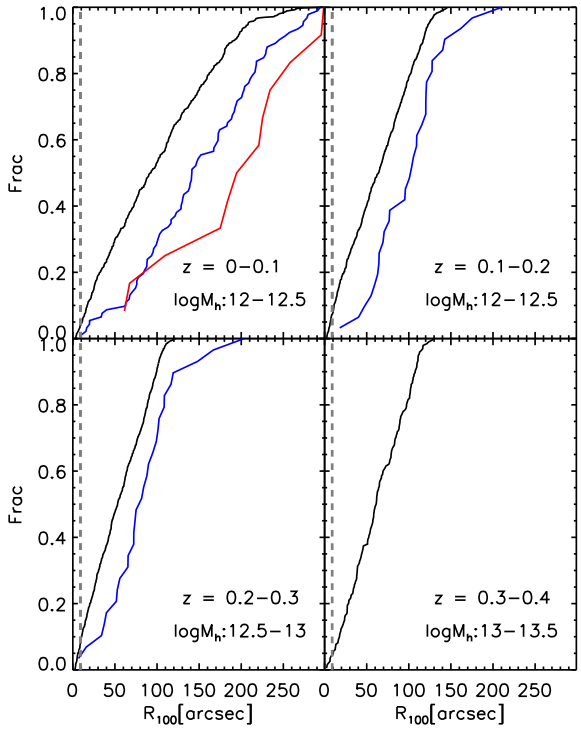

Figure 1. Cumulative distribution of groups as a function of R_{100}, the angular radius of the most distant group member from the group centre. Redshift ranges and mass ranges for the groups are indicated in the bottom-right corner of each panel. Black, blue, and red curves are for groups with optical multiplicity 2, 3, and >3, respectively. The vertical grey dashed curves in each panel indicate the *Herschel* beam radius of 9 arcsec at 250 μm.

To *k*-correct the observed 250 μm flux to the rest frame 250 μm luminosity, we assume the dust emission the Spectral Energy Distribution (SED) is a modified blackbody, as in Guo et al. (2011a):

$$L_\nu \propto B_\nu(T)\nu^\beta, \quad (1)$$

where $B_\nu(T)$ is the Planck function, and we assume $\beta = 1.5$ and fit the temperature using as many far-IR bands as are detected. We then calculate the *k*-correction for each source using its individually estimated temperature.

The median temperature of our sample is 26 K. For this assumed SED shape and temperature, the ratio of the total IR luminosity $L_{\rm IR}$ (integrated over 8–1000 μm) to $\nu{\rm L}_\nu$(250, rest frame) is 5.5 for the median temperature, so we have the conversion between monochromatic and total IR luminosities of

$$L_{\rm IR}/{\rm L}_\odot = 1.8 \times 10^{10}\, L_\nu(250\,\mu{\rm m})/(10^{24}\,{\rm W\,Hz^{-1}}). \quad (2)$$

To relate far-IR luminosities to dust-obscured SFRs, we use the relation derived by Kennicutt (1998), multiplied by 0.63 which corresponds to a Chabrier (2003) initial mass function (IMF) over

a stellar mass range $0.1 < m < 100\,\mathrm{M}_\odot$. This gives

$$\mathrm{SFR}/(\mathrm{M}_\odot\,\mathrm{yr}^{-1}) = 2.8\times10^{-44} L_{\mathrm{IR}}/(\mathrm{erg\,s^{-1}}) = 1.8\,L_\nu(250\,\mu\mathrm{m})/(10^{24}\,\mathrm{W\,Hz^{-1}}), \quad (3)$$

where in the second line we have assumed the SED shape described above with $T = 26$ K.

The conversation from $L_{250\,\mu\mathrm{m}}$ to the SFR above is only to illustrate the typical SFR. In practice, when calculating the SFR in Section 4, we use the temperature for each source from fitting its own SED. Note that L_{IR} could be underestimated with the assumption of a single modified blackbody for the SED fitting, given that the SED of dust emission could be more complicated and there are contributions from hot dust, polycyclic aromatic hydrocarbon, and very small grains (VSG) which emit in the mid-IR. The true total emission from 8 to 1000 μm could be higher by around 30–50 per cent than that obtained using equation (2). On the other hand, since a lot of the dust in H-ATLAS sources seem to be heated by older stars and not recent SFR, the conversation from the total L_{IR} in equation (3) could overestimate the derived SFR. These two effects partly compensate each other and our results should be robust within a factor of 2.

2.3 Methods for measuring the far-IR LF of galaxy groups

We use two independent methods to estimate the abundance of group/cluster galaxies as a function of their far-IR luminosity.

2.3.1 Direct matching method

Our first method (hereafter, the direct method) uses the matched H-ATLAS-GAMA galaxy catalogue. The GAMA group catalogue (Robotham et al. 2011) lists the GAMA galaxies in each GAMA group/cluster. The direct matching catalogue, on the other hand, establishes the link between the H-ATLAS source and the *r*-band selected GAMA galaxy. The combination of these two directly links the GAMA group/cluster with its H-ATLAS members. Around 33 per cent of the galaxies in the matched H-ATLAS-GAMA catalogue are identified as group members, the same as the corresponding fraction of GAMA galaxies (34 per cent).

The mean far-IR LF of galaxies in groups in a certain mass and redshift range is calculated using

$$\Phi(L_i)\,\Delta\log L_i = \frac{\Sigma_{j=0}^{N_{\mathrm{group}}} n_{i,j}}{\Sigma_{j=0}^{N_{\mathrm{group}}} N_{i,j}}, \quad (4)$$

where $\Phi(L_i)\,\Delta\log L_i$ is the number of galaxies per group in the ith luminosity bin L_i, $n_{i,j}$ is the number of matched galaxies in the ith luminosity bin for the jth group, and N_{group} is the total number of groups for a given redshift bin and group mass bin. The factor $N_{i,j}$ specifies whether the jth group contributes to the measurement in the ith luminosity bin, given the far-IR flux limit and redshift, and is defined as $N_{i,j} = 1$ if a galaxy of the ith luminosity could be detected at the redshift of the jth group, otherwise $N_{i,j} = 0$.

This method, however, might suffer some problems. Not every H-ATLAS galaxy has an optical counterpart in GAMA, even if they lie in the same redshift range and sky region. It is possible that the dust extinction is very large so that the galaxies are too faint in the *r* band to be included in GAMA. It is also possible that a high-redshift H-ATLAS galaxy is projected on to a relatively dense region in the *r*-band selected galaxy survey so that an optical counterpart is incorrectly assigned to it. When there are multiple optical candidates for a given H-ATLAS galaxy, it is also possible that the galaxy is removed from the sample due to the optical ID being ambiguous. For these reasons, we also apply an alternative method described next.

2.3.2 Stacking method

Our second method (hereafter, the stacking method) is to count the number of H-ATLAS sources within a projected radius of each GAMA group, after subtracting the local background H-ATLAS source density. Note that for this method we do not require the H-ATLAS sources to have optical counterparts in SDSS. Each H-ATLAS source is assigned the redshift of the target group to calculate its luminosity and projected separation. The far-IR LF in groups is then calculated using

$$\Phi(L_i)\,\Delta\log L_i = \frac{\Sigma_{j=0}^{N_{\mathrm{group}}}[n_{i,j}(R_j) - n_{\mathrm{bg},i}\times A_j]}{\Sigma_{j=0}^{N_{\mathrm{group}}} N_{i,j}}, \quad (5)$$

where $n_{i,j}(R_j)$ is the total number of H-ATLAS sources in the ith luminosity bin and within a projected radius R_j of the centre of the jth group (the choice of R_j will be discussed below), $n_{\mathrm{bg},ij}$ is the background surface density of H-ATLAS sources in the ith luminosity bin around the jth group (when placed at the redshift of the group), and A_j is the area enclosed by radius R_j.

A shortcoming of this method is that it relies on the choice of the radius R within which H-ATLAS sources are counted as group members. Ideally, one would use the virial radius of the group. The GAMA group catalogue provides several measures of group radius, R_{50}, $R_{1\sigma}$, and R_{100}, which are defined, respectively, as the radius of the 50th and 68th percentile and the most distant group member from the central galaxy. It is possible that even the most distant projected member is still well within the virial radius. It is beyond the scope of this paper to investigate how well different observational definitions of group radius reflect the 'real' group radius. Here, we adopt R_{100} as the default radius R.

Another potential drawback of this method is that we need to estimate the local background surface density n_{bg} of H-ATLAS sources around each group. We do this by counting sources in annuli around each group. It is possible that the background surface density could be over or underestimated if there is an over or underdense region along the line of sight to the target group/cluster even though it is unbiased on average. We tested how sensitive our results might be to this effect by varying the inner and outer radii of the annuli used to measure the local background. We find that our results are insensitive to the exact choice of these radii (see Appendix A). Hereafter, we use annuli of radii $R_{100} < R < 3R_{100}$ around each group to measure the local background density n_{bg}.

3 GROUP LUMINOSITY FUNCTIONS

In this section, we first study the rest-frame 250 μm LF for all galaxies, and then the conditional 250 μm LF in galaxy groups of different masses and at different redshifts. We fit these LFs with an analytical function, and use this to study the dependence of characteristic luminosity on group mass and redshift, as well as the contribution to the overall 250 μm luminosity density from haloes of different masses at different redshifts.

3.1 Far-IR luminosity function in the field

In order to have a better understanding of our results for the far-IR galaxy LF in different galaxy environments, we start by measuring the 250 μm field LF using all galaxies in our matched H-ATLAS-GAMA sample with spectroscopic redshifts. 'Field' galaxies

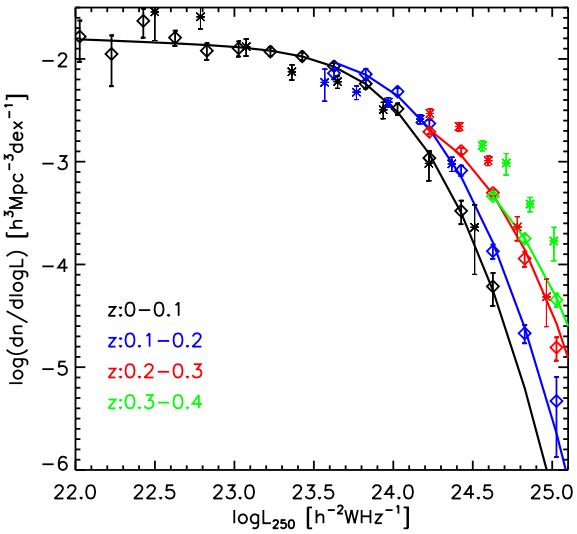

Figure 2. The far-IR LF of field galaxies at 250 μm. The different colours indicate different redshifts, as shown in the key. Diamonds with different colours are our results. The curves with corresponding colours are the fits to our data using equation (6). The stars show the results from Dye et al. (2010), as discussed in the text.

include galaxies in all environments. We use the $V_{\rm max}$ estimator (e.g. Felten 1976; Avni & Bahcall 1980), where the maximum volume $V_{\rm max}$ within which a galaxy would be detected is calculated by combining the far-IR ($S_\nu(250) > 35$ mJy) and optical ($r < 19.4$) flux limits. We calculate the *k*-corrections for the *r*-band using the procedure in Robotham et al. (2011). We calculate the LF, defined as the number of galaxies per unit volume per dex in luminosity, in four redshift bins over $0 < z < 0.4$. Our results are shown in Fig. 2 (diamonds with errorbars), where different colours show different redshifts. We estimate errorbars using the jackknife method, dividing the full sample into 10 subsamples. We find strong evolution in the 250 μm LF even at these low redshifts, in broad agreement with earlier work using only *Herschel* Science Demonstration Phase (SDP) data (Dye et al. 2010; Eales et al. 2010b).

We have made a detailed comparison with the results of Dye et al. (2010), who used H-ATLAS SDP data with a similar 250 μm flux limit, but covering only 16 deg^2. Dye et al.'s measurements are plotted as stars in Fig. 2, for the same redshift intervals as we use. We see that our results are in good agreement with Dye et al. for the two lowest redshift bins at $z < 0.2$, but differences start to appear in the redshift bin $0.2 < z < 0.3$ and become large in our highest redshift bin $0.3 < z < 0.4$, in the sense that we find weaker evolution than Dye et al. at the bright end of the LF. We have identified two main reasons for these differences: (i) Dye et al.'s sample includes H-ATLAS galaxies with fainter optical counterparts ($r < 22.4$) than ours ($r < 19.4$). This forces Dye et al. to use less accurate photometric redshifts for most of his sample, with spectroscopic redshifts only for a minority of galaxies. While the $V_{\rm max}$ method should automatically allow for the difference in *r*-band magnitude limits between our sample and his in the case of a uniform galaxy distribution, the strong redshift evolution of the LF breaks this assumption. Examining our highest redshift bin, $0.3 < z < 0.4$, we find that our $r < 19.4$ H-ATLAS sample with spectroscopic redshfit has redshifts concentrated at the lower end of this range, while a $r < 22.4$ H-ATLAS sample with photo-*z* covers the whole redshift bin. Due to the evolution in density across the redshift bin, the $V_{\rm max}$ method then underestimates the mean LF in the redshift bin when we use our $r < 19.4$ sample. (ii) Cosmic variance also contributes to the differences between Dye et al.'s LFs and ours, since we use the H-ATLAS Phase I catalogue, which covers a much larger area than the SDP field used in Dye et al. This allows us to measure the LF to lower far-IR luminosities in the lowest redshift bin ($0 < z < 0.1$). (iii) Source completeness could also affect the measured LFs. There are three sources of incompleteness. One is the far-IR incompleteness. Rigby et al. (2011) found that for the flux cut adopted in this work, 35 mJy, the catalogue is >80 per cent complete. The second is the optical catalogue incompleteness. Dunne et al. (2011) found that at $r < 21.6$ the optical catalogue is 91.1 per cent complete. For our study, we use 19.4 as the *r*-band magnitude cut, from which the completeness is even higher than this value. The last source of incompleteness is from the matching *Herschel* sources to optical galaxies. For our samples of $S_{250\mu\rm m} > 35$ mJy and $r < 19.4$, around 80 per cent of the H-ATLAS sources have reliable matches (Smith et al. 2011, and private communication). We find that the effect (i) dominates the differences between our LF and Dye et al.'s in the $z = 0.3-0.4$ redshift bin, while effect (ii) is the main source of differences up to $z = 0.3$. Effect (iii) mainly matters for the faint end of the LFs at $z > 0.2$.

Table 1. Best-fitting LF parameters for the 250 μm field LF at different redshifts, using equation (6). α and σ are fixed using the fit at $z = 0-0.1$.

Redshift	α	σ	$\log\phi^*(h^3{\rm Mpc}^{-3}{\rm dex}^{-1})$	$\log {\rm L}^*(h^{-2}{\rm WHz}^{-1})$
0–0.1	1.06	0.30	−1.91±0.04	23.70±0.07
0.1–0.2	1.06	0.30	−1.94±0.06	23.83±0.04
0.2–0.3	1.06	0.30	−2.39±0.05	24.14±0.03
0.3–0.4	1.06	0.30	−2.72±0.04	24.30±0.03

It is convenient to describe the measured LF by an analytic fit. We use the modified Schechter function originally proposed by Saunders et al. (1990) to fit the far-IR LF at 60 μm, which has a more gradual decline at high luminosity than a Schechter function:

$$\phi(L) \equiv \frac{{\rm dn}}{{\rm dlog}_{10}L} = \phi^* \left(\frac{L}{L^*}\right)^{1-\alpha} \exp\left[-\frac{1}{2\sigma^2}\log_{10}^2\left(1+\frac{L}{L^*}\right)\right]. \quad (6)$$

In this function, *n* is the number density of galaxies, α determines the slope at the faint end, σ controls the shape of the cutoff at the bright end, L^* is the characteristic luminosity, and ϕ^* is the characteristic density. We have fitted this function to our measured LF in each redshift bin, and the resulting parameters are listed in Table 1. We have fixed the shape parameters α and σ at the best-fit values for the $z = 0-0.1$ redshift bin, since our measurements at higher redshifts do not cover a wide enough luminosity range to robustly determine all four parameters in equation (6). We find that the characteristic luminosity for the $z = 0-0.1$ bin is $L^*(250) = 10^{23.67}\,h^{-2}\,{\rm W\,Hz^{-1}}$, which corresponds to a total IR luminosity $L_{\rm IR} = 1.0 \times 10^{10}\,h^{-2}\,{\rm L}_\odot$. Using equation (3), this corresponds to a dust-obscured SFR $= 1.1\,h^{-2}\,{\rm M}_\odot\,{\rm yr}^{-1}$. Based on our fits, $L^*(250)$ increases rapidly with redshift, being about three times larger at $z = 0.35$ compared to $z = 0.05$. The characteristic density ϕ^* also changes rapidly with redshift, falling by a factor of 7 over the same redshift range.

3.2 Far-IR luminosity function in groups

We begin our analysis of the far-IR CLF in galaxy groups by comparing results obtained using the two methods described in Section 2.3, the direct method and the stacking method. We split our sample according to group mass and redshift, in order to separate environmental effects from redshift evolution. The results are shown

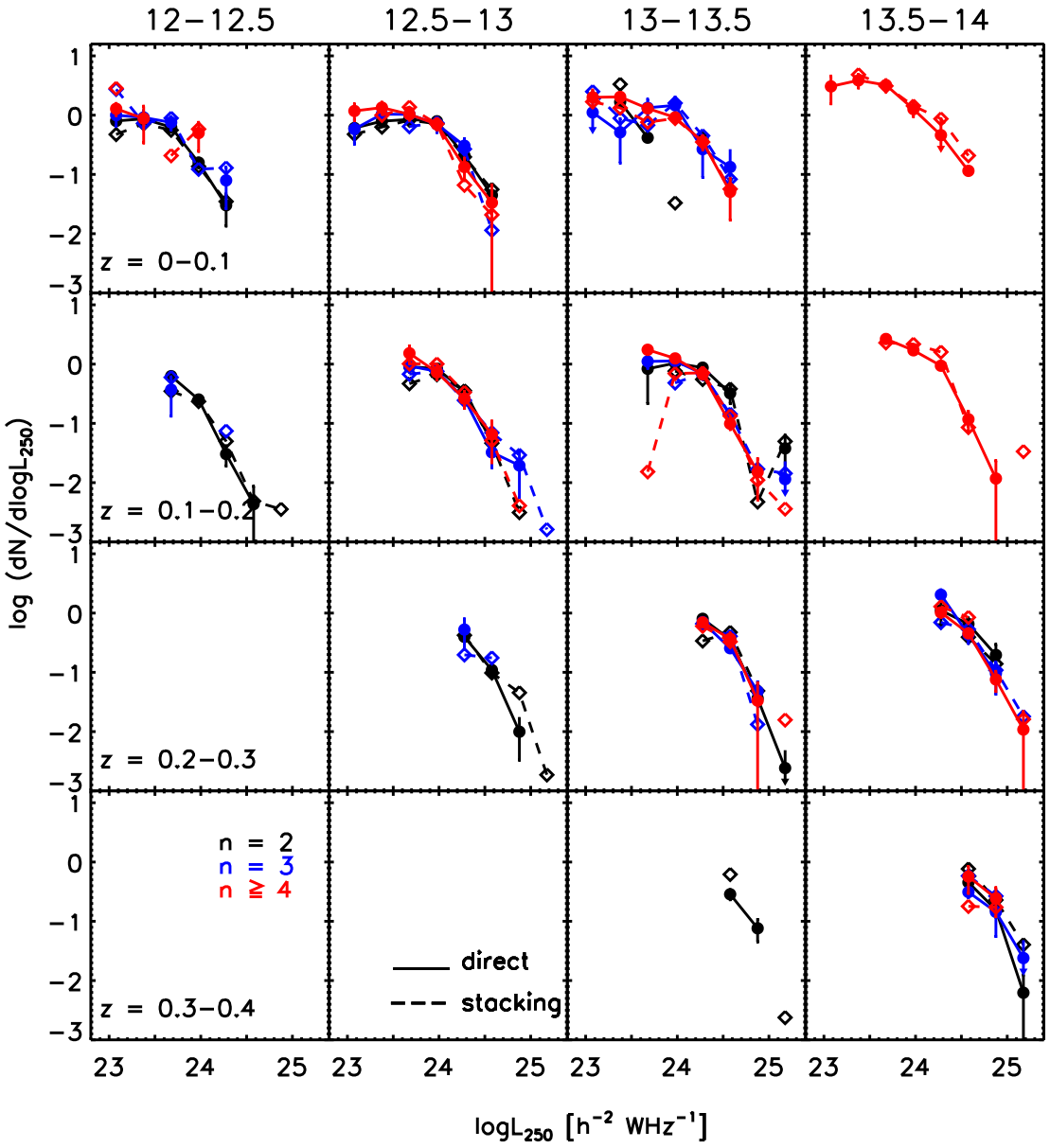

Figure 3. Group far-IR conditional luminosity function (defined as mean number of galaxies per group) at 250 μm as a function of halo mass (left to right) and redshift (top to bottom). The redshift range is indicated in the left-hand panels, and the logarithm of the group halo mass in $h^{-1}\,M_{\odot}$ above the top panels. Solid curves with filled circles show results from the direct method, and dashed curves with empty diamonds from the stacking method. For clarity, errorbars are plotted only for the direct method. The different colours are for groups of different optical multiplicities, n: black for multiplicity n =2, blue for n =3 and red for $n \geq 4$. Errorbars which extend down to 0 are indicated with downward arrows.

in Fig. 3, with the direct method shown by solid lines and the stacking method by dashed lines. We have estimated errorbars using the jackknife method. We have also checked for any dependence of the CLFs on the group optical multiplicity n, defined as the number of r-band selected galaxies with spectroscopic redshifts which define this group in the GAMA group catalogue. The multiplicity n is relevant both for the estimate of the group radius (which is important for the stacking method) and for the estimate of the group mass. We thus further split our group samples according to their multiplicities. Results for different multiplicities are shown by different colours (black: $n = 2$, blue: $n = 3$, and red: $n \geq 4$). For groups of a given mass, redshift range, and multiplicity, Fig. 3 shows that the LFs estimated using the direct and stacking methods are consistent. Since the results from the stacking method are independent of the optical ID matching used in the direct method, the consistency between the CLFs obtained by the two methods demonstrates that the direct method does not miss a significant fraction of H-ATLAS galaxies due to there being either multiple optical candidates for a given H-ATLAS galaxy, or no counterparts brighter than $r < 19.4$. However, the results from the stacking method are much noisier, which appears to be due mostly to uncertainties in the background subtraction. We therefore use only results from the direct method in the analysis that follows. We also find that for both methods, the inferred group LFs depend only weakly on the optical multiplicities. In the following analysis, we therefore use all groups (i.e. multiplicity $n \geq 2$) in order to have better statistics, unless indicated otherwise. We see that CLFs can be measured over quite a wide range of group halo mass ($10^{12}-10^{14}\,h^{-1}\,M_{\odot}$) for $z < 0.2$, though

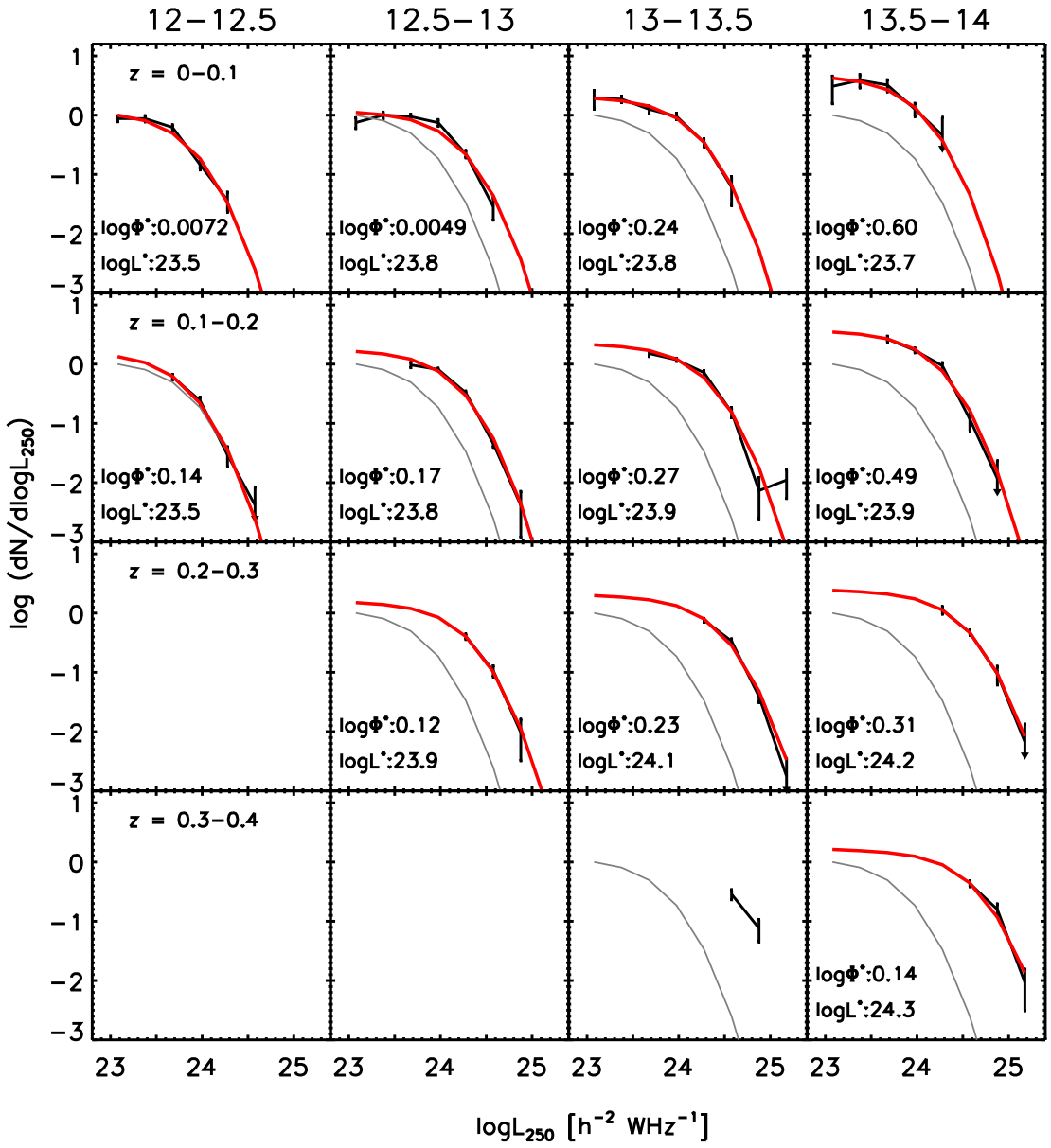

Figure 4. Far-IR luminosity functions of galaxies in groups. Black curves with errorbars are the direct measurement for optical multiplicity $n \geq 2$, and red curves are the analytic fits. The parameters α and σ in equation (6) are fixed to 1.06 and 0.30 as measured for the field luminosity function at $z = 0$–0.1. The other two parameters encoding the characteristic luminosity L^* (in units of $h^{-2}\,\mathrm{W\,Hz^{-1}}$) and the amplitude of the luminosity functions Φ^* are indicated in the lower-left corner of each panel. The redshift range is indicated in the left-hand panels, and the logarithm of the group halo mass in $h^{-1}\,\mathrm{M}_\odot$ above the top panels. The fit in the top-left panel is replicated as a grey curve in all the other panels as a reference.

this range shrinks with redshift, so that in the highest-redshift bin we can measure LFs only in the most massive groups.

3.3 Characteristic properties of the far-IR luminosity function in groups

In order to study the dependence of the far-IR LF on group mass and redshift, it is convenient to fit the measured CLFs with an analytical function. We use the same modified Schechter function as in equation (6), except with Φ, the mean number of galaxies per group per $\log_{10}L$, replacing ϕ, the mean number of galaxies per unit volume per $\log_{10}L$, and correspondingly Φ^* replacing ϕ^*. Since our measured CLFs mostly do not cover a wide enough range in luminosity to reliably constrain all four parameters (α, σ, Φ^*, and L^*) in the fit, we fix the shape parameters at the values $\alpha = 1.06$ and $\sigma = 0.30$ which we measure for the $z = 0$–0.1 field LF, and then fit Φ^* and L^* independently for each bin in group mass and redshift. The resulting fits are shown in Fig. 4, where the black curves with errorbars show the direct measurements, while the red curves show the fits. The measured CLF for the mass range of 10^{13}–$10^{13.5}$ and redshift range $z = 0.3$–0.4 has only two data points, so we do not try to fit this with our analytic function. It can be seen that the functional form of equation (6) provides a good fit to our measured CLFs for all mass and redshift ranges for which we have data. To show the dependence of the CLF on group mass and redshift more clearly, we also repeat the fit from the top-left panel ($z = 0$–0.1 and $M_\mathrm{h} = 10^{12}$–$10^{12.5}\,h^{-1}\,\mathrm{M}_\odot$) as a grey line in the other panels. This shows that the CLF tends to increase with both group mass

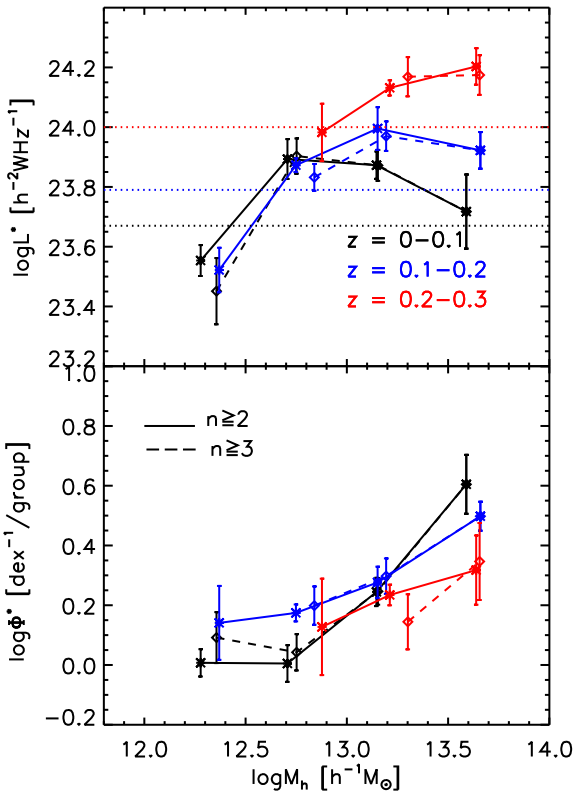

Figure 5. Top panel: characteristic luminosity, L^*, as a function of group mass and redshift. Different colours show different redshift bins, as indicated by the legend. The crosses and solid lines show results for optical multiplicity $n \geq 2$, and open diamonds and dashed lines for $n \geq 3$. The errorbars show jackknife errors. the dotted horizontal lines show L^* for the field luminosity function at the same redshifts. Bottom panel: normalization Φ^* as a function of group mass and redshift. In both panels, data are plotted at the median value of group mass for that bin.

and redshift. The far-IR multiplicity, measured by the number of galaxies with $L_{250} > 10^{23.5}\,h^{-2}\,\mathrm{W\,Hz^{-1}}$ is around unity in the least massive groups in our sample.

We show the dependence of the CLF parameters L^* and Φ^* on group mass and redshift in the top and bottom panels of Fig. 5. (We omit the results for the redshift bin $z = 0.3{-}0.4$ from this and the following plots, since we have only measured the CLF for two bins in group mass for this case.) The solid lines show results for group optical multiplicity $n \geq 2$ and the dashed lines for $n \geq 3$. We see that the results for different multiplicity cuts are generally consistent for both L^* and Φ^*.

Examining first the dependence of L^* on group mass, we see that for $z < 0.2$, it increases steeply with group mass at low masses, but then appears to turn over to a gradual decline at high masses, although the large errorbars on L^* for high masses make it difficult to be certain about the decline. Note that the estimated completeness of the group catalogue for the lowest mass range is rather low, ∼45 per cent and 20 per cent at $0<z<0.1$ and $0.1<z<0.2$, respectively. This might lead to an overestimation of the dependence on group mass at these masses. For $0.2 < z < 0.3$, only groups more massive than $\sim 10^{12.5}\,h^{-1}\,\mathrm{M_\odot}$ are detected in H-ATLAS-GAMA. For this redshift range, the measured L^* increases monotonically with group mass, though appearing to flatten at the highest masses.

The redshift evolution of L^* thus depends strongly on the group mass. For the highest masses sampled, $M_\mathrm{h} \sim 10^{13.75}\,h^{-1}\,\mathrm{M_\odot}$ (i.e. clusters), L^* increases by a factor of 2–3 over the range $0.05 < z < 0.35$, while for more typical groups, with $M_\mathrm{h} \sim 10^{12.75}\,h^{-1}\,\mathrm{M_\odot}$, there is almost no evolution for $0.05 < z < 0.25$.

In the top panel of Fig. 5, we also overplot as horizontal dotted lines the values of L^* which we measure for the field LF at the same redshifts. We see that L^* for field galaxies always lies between the values in the least and the most massive groups, consistent with the finding in previous work that most H-ATLAS galaxies resides in groups of mass comparable to the Milky Way halo (Guo et al. 2011b).

In the bottom panel of Fig. 5, we show how the CLF normalization Φ^* varies as a function of group mass at different redshifts. We again see that the redshift evolution depends on group mass. For lower mass groups ($M_\mathrm{h} \sim 10^{12.25}$–$10^{12.75}\,h^{-1}\,\mathrm{M_\odot}$), Φ^* increases with redshift for $z < 0.2$, while for the highest masses ($M_\mathrm{h} \sim 10^{13.75}\,h^{-1}\,\mathrm{M_\odot}$), it appears instead to decrease with increasing redshift for $z \lesssim 0.3$, although the large errorbars in the latter case make it difficult to be certain about the behaviour.

3.4 Far-IR luminosity-to-mass ratio of groups and the far-IR luminosity density

A further important physical quantity which we can calculate from our measured group far-IR CLFs is the total far-IR luminosity-to-mass ratio of groups, since this is related to the dust-obscured SFR per unit dark halo mass. Previous studies have found that the fraction of star-forming galaxies decreases with group mass (e.g. Dressler 1980; Kimm et al. 2009). However, direct measurements of SFR per group mass are very rare because the determination of the SFR depends greatly on corrections for dust extinction when using UV and optical tracers, and also because it is not trivial to measure group masses for large samples.

Here, we integrate our analytic fits to the group CLFs shown in Fig. 4 over luminosity to estimate the average total 250 μm luminosity $L_{250,\mathrm{tot}}$ for groups in each mass and redshift range, and hence obtain the 250 μm luminosity-to-mass ratios of groups. Since we have not directly measured the group CLFs at $L_{250} < 10^{23}\,h^{-2}\,\mathrm{W\,Hz^{-1}}$, but instead simply assumed the same faint-end slope α as we measured for the field 250 μm LF at $z < 0.1$, we calculate the total group luminosities $L_{250,\mathrm{tot}}$ using two different lower limits of integration, $L_{250,\mathrm{min}} = 0$ and $10^{23.5}\,h^{-2}\,\mathrm{W\,Hz^{-1}}$. The values of total luminosity drop by a factor of up to 1.5 when using the higher luminosity cut. Our results for the luminosity-to-mass ratios $L_{250,\mathrm{tot}}/M_\mathrm{h}$ for $L_{250,\mathrm{min}} = 0$ are shown in the left-hand panel of Fig. 6. As in Fig. 5, the solid lines show results for group optical multiplicity $n \geq 2$, and dashed lines are for $n \geq 3$, from which we see that our estimates of $L_{250,\mathrm{tot}}/M_\mathrm{h}$ are insensitive to optical multiplicity. We also note that there is some degeneracy between our fitted values of L^* and Φ^* in the group CLFs, but the effects of this are partly removed when we calculate the luminosity-to-mass ratios, which is reflected in the size of the errorbars plotted in Fig. 6.

Fig. 6 shows that at each redshift, the 250 μm luminosity-to-mass ratio is a decreasing function of the group mass. At $z = 0$, the maximum $L_{250,\mathrm{tot}}/M_\mathrm{h}$ is $\sim 10^{11.2}\,h^{-2}\,\mathrm{W\,Hz^{-1}}$ in groups with masses $\sim 10^{12.3}\,h^{-1}\,\mathrm{M_\odot}$, comparable to the Milky Way halo, and decreases to $\sim 10^{10.5}\,h^{-2}\,\mathrm{W\,Hz^{-1}}$ for groups of mass $\sim 10^{13.5}\,h^{-1}\,\mathrm{M_\odot}$. This implies a decreasing rate per unit mass for converting baryons to stars through dust-obscured star formation with increasing group mass. The dependence of $L_{250,\mathrm{tot}}/M_\mathrm{h}$ on group mass can be fitted by a power law except at the very low mass end, where the slope becomes flatter. At higher redshift, the $L_{250,\mathrm{tot}}/M_\mathrm{h}$ versus M_h relation shares the same slope as that at $z = 0$, while its amplitude

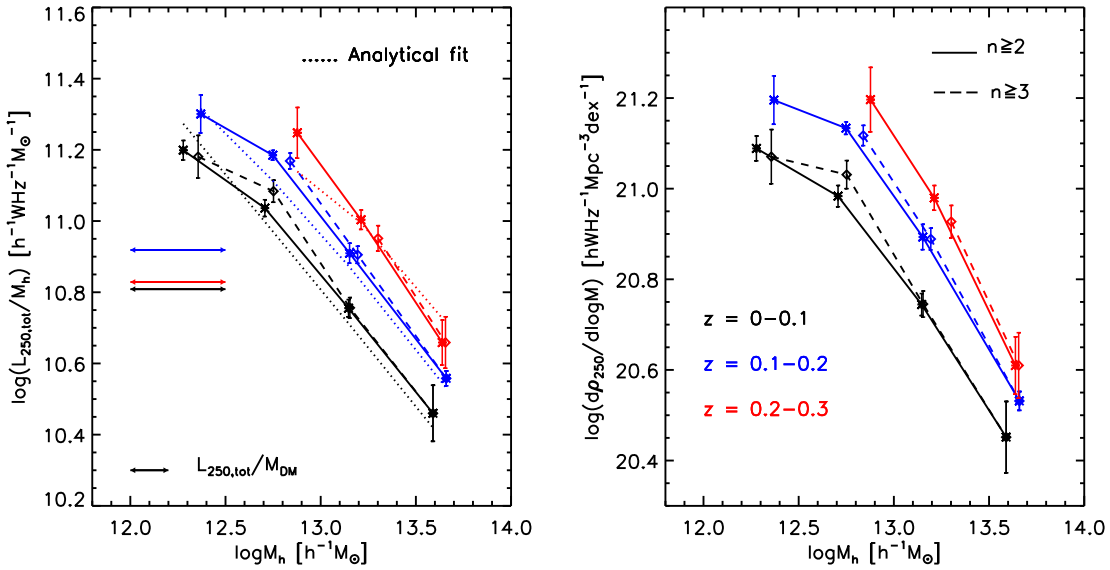

Figure 6. Left panel: the ratio of the total far-IR luminosity at 250 μm to total group mass as a function of group mass and redshift. Right panel: contribution to the far-IR (250 μm) luminosity density from haloes of different mass. In both panels, different colours are for different redshift ranges, errorbars are estimated using the jackknife technique, and solid and dashed lines are for group optical multiplicity $n \geq 2$ and $n \geq 3$, respectively. The dotted lines in the left-hand panel show the analytic fit, equation (7), evaluated at the median mass and redshift for each bin. In both panels, data are plotted at the median value of group mass for that bin in $\log M_{\rm h}$ and redshift. The horizontal lines in the left-hand panel show the ratio of 250 μm luminosity density to dark matter density for the whole galaxy population, calculated from the field 250 μm LF.

increases significantly with redshift. Specifically, the amplitude increases by about a factor of 3 from $z \approx 0.05$ to $z \approx 0.35$. We fit this luminosity-to-mass ratio as a function of group mass and redshift with the following equation:

$$\frac{L_{250,\rm tot}}{M_{\rm h}} = 10^{11.3\pm0.3}(1+z)^{4.74\pm0.41}\left(\frac{M_{\rm h}}{10^{12}\,h^{-1}\,{\rm M}_\odot}\right)^{-0.65\pm0.02}. \quad (7)$$

This analytic fit is shown by dotted lines in the left-hand panel of Fig. 6, where it is evaluated and plotted for the median mass and redshift of the groups in each bin. While the luminosity-to-mass ratio $L_{250,\rm tot}/M_{\rm h}$ decreases with group mass, the far-IR luminosity increases with mass roughly as $L_{250,\rm tot} \propto M_{\rm h}^{0.35}$ over the range of mass $10^{12} < M_{\rm h} < 10^{14}\,h^{-1}\,{\rm M}_\odot$ probed in this study.

The horizontal lines in the left-hand panel of Fig. 6 show the mean luminosity-to-mass ratio $L_{250,\rm tot}/M_{\rm DM}$ for the galaxy population as a whole at the same redshifts, obtained by integrating over the field LF and dividing by the cosmological dark matter density. We see that $L_{250,\rm tot}/M_{DM}$ in the field increases with redshift in a similar way to that in groups between the two lowest redshift bins, but then drops in the $z = 0.2$–0.3 bin. This drop may be caused by errors in our estimate of the field LF in this redshift range, as discussed in Section 3.1.

Finally, we combine our measurement of the far-IR luminosity-to-mass ratios of groups with a theoretical prediction for the number density of haloes as a function of mass to estimate the contribution to the far-IR luminosity density at 250 μm, ρ_{250}, from groups of different masses:

$$\frac{{\rm d}\rho_{250}}{{\rm d}\log M_{\rm h}} = \left(\frac{L_{250,\rm tot}}{M_{\rm h}}\right) M_{\rm h} \left(\frac{{\rm d}n}{{\rm d}\log M_{\rm h}}\right). \quad (8)$$

In the above formula, we use the theoretically predicted dark matter halo mass function ${\rm d}n/{\rm d}\log M_{\rm h}$ in a standard ΛCDM cosmology, specifically, the analytical mass function of Reed et al. (2007), which has been shown to match N-body simulations very well. We also use the directly measured values of $L_{250,\rm tot}/M_{\rm h}$ for each bin in mass and redshift, rather than the analytical fit in equation (7).

The right-hand panel of Fig. 6 shows the resulting estimate of the contribution to the 250 μm luminosity density ρ_{250} from groups of different mass. As in the left-hand panel, results are split into different redshift bins. We find that the total far-IR luminosity density contributed by haloes of different masses is a decreasing function of halo mass. For those more massive than $10^{12.5}\,h^{-1}\,{\rm M}_\odot$, the far-IR luminosity density can be fitted with a power law, while the slope gets flatter for lower masses at $z < 0.2$, where we still have measurements for such low masses. The 250 μm luminosity density increases with redshift at all group masses. This behaviour is very similar to that of the luminosity-to-mass ratio, which is expected since the evolution of the dark matter halo mass function in this redshift range is quite weak. As before, we find that our results are insensitive to whether we use groups with optical multiplicity $n \geq 2$ or $n \geq 3$.

For completeness, we also derive the total far-IR luminosity density ρ_{250} by integrating over our measured field galaxy LF, and report our results in Table 2. We also report there our estimates of the contributions to the total luminosity density from groups in the mass ranges probed by the H-ATLAS-GAMA survey. We give values of ρ_{250} for two different lower limits for the integrations over L_{250}, $L_{250,\rm min} = 0$ and $10^{23.5}\,h^{-2}\,{\rm W\,Hz^{-1}}$. We find that whichever of these luminosity cuts we adopt, groups more massive than $10^{12}\,h^{-1}\,{\rm M}_\odot$ contribute around 70 per cent of the total luminosity density at $z < 0.2$. For $0.2 < z < 0.3$, groups more massive than $10^{12.5}\,h^{-1}\,{\rm M}_\odot$ already contribute nearly 70 per cent of the total.

3.5 Comparison with previous work

Previous direct measurements of the IR LFs of galaxy groups and clusters are quite limited. Bai et al. (2006, 2007, 2009) used mid-IR (*Spitzer* 24 μm) data to measure the IR LFs of several rich clusters ($M \sim 10^{15}\,{\rm M}_\odot$) at $z \lesssim 1$ and found strong redshift evolution in

Table 2. Integrated 250 μm luminosity density from the field and from groups as a function of redshift. The first column is the redshift range. The second and the third columns give the total luminosity density in the field from integrating our analytic fit down to $L_{250,\rm min} = 0$ and $10^{23.5}\,h^{-2}\,{\rm W\,Hz^{-1}}$, respectively. The fourth column gives the ranges of group halo mass probed in our study. The fifth and sixth columns give the contributions to the total luminosity density from groups in these mass ranges, using the same two lower luminosity cuts as for the field. The percentages give the fractions of the corresponding field luminosity density for the same lower luminosity cut. Halo masses are given in units $h^{-1}\,{\rm M_\odot}$ and luminosity densities in units $h\,{\rm W\,Hz^{-1}\,Mpc^{-3}}$.

Redshift	Field	Field ($>10^{23.5}$)	log $M_{\rm h}$	Group	Group ($>10^{23.5}$)
0–0.1	$10^{21.65}$	$10^{21.45}$	>12	$10^{21.48}$ (68 per cent)	$10^{21.30}$ (70 per cent)
0.1–0.2	$10^{21.75}$	$10^{21.60}$	>12	$10^{21.60}$ (71 per cent)	$10^{21.43}$ (67 per cent)
0.2–0.3	$10^{21.72}$	$10^{21.64}$	>12.5	$10^{21.46}$ (55 per cent)	$10^{21.38}$ (55 per cent)

L_*, as also found in the field (e.g. Le Floc'h et al. 2005), but no dependence on radius within a cluster. They also found that the shape of the IR LF in clusters was similar to that in the field at the same redshift, a result confirmed by Finn et al. (2010), who studied 16 clusters drawn from the ESO Distant Cluster Survey at $0.4<z<0.8$. This is however, in contrast to what was found by Goto et al. (2010), who used the *AKARI* 8 μm observations of a single rich cluster at $z\sim0.8$, and found that L_* is lower by a factor of 2.4 compared to the field at the same redshift. Comparing with our results, Fig. 5 shows that in clusters with $M_{\rm h}\sim10^{14}\,{\rm M_\odot}$, L_* differs by less than 50 per cent from the field value, while the difference can be larger at lower group masses.

Hα is another important tracer of the SFR. The Hα LFs of rich clusters have been measured in various studies, and generally been found to have similar shapes to that of the field population at the same redshift (e.g. Balogh et al. 2002; Kodama et al. 2004). This is similar to the result for IR LFs. In a related result, Giodini et al. (2012) measured the stellar mass function of star-forming galaxies in galaxy groups with $10^{13}\lesssim M\lesssim10^{14}\,{\rm M_\odot}$ at $0.2<z<1$, and found that it has a similar shape to that for the field.

As discussed above, $L_{\rm IR,tot}/M_{\rm h}$ is an indicator of the total dust-obscured SFR (summed over all galaxies) per unit halo mass. For our sample of ∼3000 galaxy groups with $10^{12}<M_{\rm h}<10^{14}\,h^{-1}\,{\rm M_\odot}$ at $z<0.4$, we find $L_{\rm IR,tot}/M_{\rm h}\propto(1+z)^5$ (see Fig. 6). This dependence is in reasonable agreement with that found in previous work from mid-IR observations of samples of clusters ($M_{\rm h}\gtrsim10^{14}\,{\rm M_\odot}$) for $0<z<1$, which found $\Sigma{\rm SFR}/M_{\rm h}\propto(1+z)^\alpha$, with $\alpha\approx5-7$ (Geach et al. 2006; Bai et al. 2007, 2009; Koyama et al. 2010; Webb et al. 2013). Based on data from the *Herschel* Multi-tiered Extragalactic survey (Oliver et al. 2010), De Bernardis & Cooray (2012) also find a similar redshift dependence, $\alpha\sim4$ for $z=0.2$–4, using a halo occupation distribution model fitting method. Our result is also similar to that found by Popesso et al. (2012) from *Herschel* far-IR (100 and 160 μm) observations of a sample of ∼20 massive groups and rich clusters ($10^{13}\lesssim M_{\rm h}\lesssim10^{15}\,{\rm M_\odot}$) at $0.1\lesssim z\lesssim1$. We note that these previous studies all estimated ΣSFR by summing IR-based SFRs over galaxies brighter than some IR luminosity limit, typically $L_{\rm IR}\gtrsim10^{11}\,{\rm L_\odot}$. In contrast, we fit the IR LFs of groups down to much fainter luminosities, and then integrate over these fits (extrapolated to $L_{\rm IR}=0$) to estimate the total group IR luminosities. Since the characteristic IR luminosity L_*, and hence the shape of the LF, evolves with redshift, these two approaches will lead to redshift evolution factors that differ in detail. Indications of similarly strong evolution of $\Sigma{\rm SFR}/M_{\rm h}$ were also found from studies using Hα-based SFRs, for small samples of clusters at $0.2\lesssim z\lesssim0.8$ (e.g. Kodama et al. 2004; Finn, Zaritsky & McCarthy 2004; Finn et al. 2005).

From our sample of galaxy groups, we also find a dependence on group mass, $L_{\rm IR,tot}/M_{\rm h}\propto M_{\rm h}^{-0.65}$. This trend is qualitatively similar to indications from previous Hα (Finn et al. 2005), mid-IR (Bai et al. 2007) and far-IR (Popesso et al. 2012) studies of galaxy clusters, although it is significantly flatter than the trend $\Sigma{\rm SFR}/M_{\rm h}\propto M^{-1.5\pm0.4}$ found by Webb et al. (2013) from mid-IR observations of a sample of clusters at $0.3<z<1$. (Note, however, that the Webb et al. estimates of $\Sigma{\rm SFR}/M_{\rm h}$ only include galaxies brighter than $L_{\rm IR}>2\times10^{11}\,{\rm L_\odot}$.) Compared to previous work, our study, although restricted to a lower redshift range, covers a much lower and wider range of group mass and a wider range of IR luminosity, as well as having much better statistics due to the larger number of groups.

4 FAR-IR-TO-OPTICAL COLOURS IN GROUPS

The far-IR emission is a good indicator for the dust-obscured SFR, since it represents the energy re-emitted by dust when heated by (mostly young) stars. On the other hand, the optical luminosity is a tracer of the stellar mass, since it includes emission from older stars. The 250 μm to *r*-band colour should therefore be a good indicator of the specific star formation rate (sSFR = SFR/$M_\star$). The dividing line between 'star-forming' and 'passive' galaxies is typically defined as sSFR $>10^{-11}-1$ (e.g. Weinmann et al. 2010). At the median redshift, $z\approx0.2$ of the matched H-ATLAS-GAMA sample, the flux limit $S_\nu(250\,\mu{\rm m})>35$mJy of our far-IR-selected sample corresponds to a dust obscured SFR $\sim4\,{\rm M_\odot}-1$. Therefore, galaxies included in our H-ATLAS-GAMAsample would typically be classed as star-forming based on their sSFR, provided they have stellar masses $\lesssim10^{11}\,{\rm M_\odot}$.

We use galaxies from our matched H-ATLAS-GAMA sample, to obtain both far-IR and the optical luminosities, and hence their far-IR-to-optical colours. We further restrict our analysis to $z<0.2$. In Fig. 7, we plot the rest-frame 250 μm-to-*r*-band luminosity ratio $(\nu_{250}L_{250})/(\nu_rL_r)$, which is an indicator of sSFR, against the *r*-band absolute magnitude, which is an indicator of stellar mass. The three panels show different redshift ranges. In each panel, the dashed black lines show the median 250 μm/*r*-band colour for all H-ATLAS-GAMA galaxies in that bin of *r*-band absolute magnitude, with the errorbars showing the 16–84 per cent range around this (equivalent to the 1σ range for a Gaussian). The coloured lines show the median colours for galaxies in groups of different masses, as indicated by the key, with the dotted lines indicating the 16–84 per cent range. The grey region in each plot indicates where our H-ATLAS-GAMA sample becomes significantly incomplete due to the 250 μm flux limit. We calculate the upper boundary of this region in each bin of absolute magnitude M_r from the 250 μm

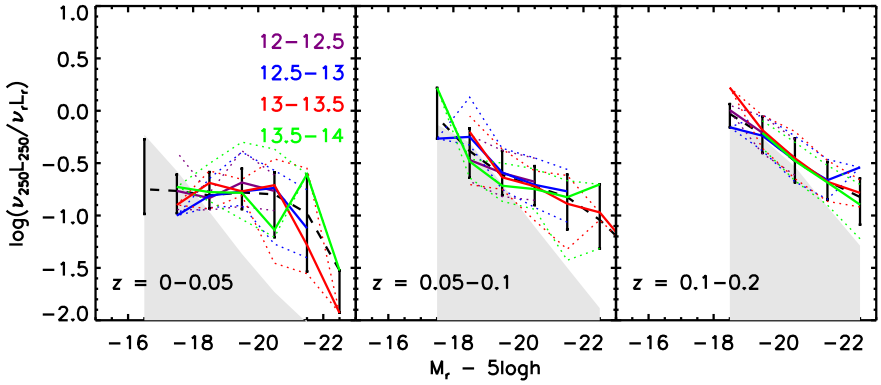

Figure 7. The far-IR-to-optical colour versus *r*-band absolute magnitude relation for different environments. The left, middle, and right panels are for redshift ranges $0 < z < 0.05$, $0.05 < z < 0.1$, and $0.1 < z < 0.2$, respectively, as labelled. The black dashed lines show the colour–magnitude relation for field galaxies in that redshift range. The coloured lines show the relation for galaxies in groups of different masses, with the logarithm of the group mass (in $h^{-1}\,\mathrm{M}_{\odot}$) being given by the key in the left-hand panel. The thick lines show the median colour, and the thin dotted lines indicate the 68 per cent range around the median. Grey regions indicate the region within which incompleteness due to the 250 μm flux limit is important.

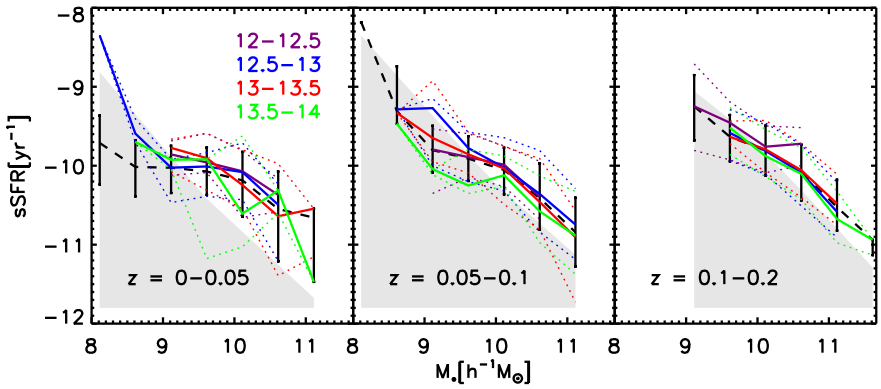

Figure 8. The specific star formation rate $\mathrm{SFR}/M_{\mathrm{star}}$ versus stellar mass M_{star}. The line type and colour coding are the same as in Fig. 7.

luminosity for a galaxy at the 250 μm flux limit at the median redshift for all GAMA galaxies in that absolute magnitude bin in that redshift range (whether they are detected at 250 μm or not), assuming a median dust temperature of 26 K. This provides only a rough estimate of the completeness boundary, since some galaxies will be at redshifts lower than the median, and so would be detected with lower 250 μm luminosities than the simple estimate above, and because the 1σ scatter in galaxy temperature could be as large as 4 K. This effect explains why the median colour–magnitude relation for faint M_r falls just inside the grey incompleteness region in the $0 < z < 0.05$ panel – in these cases, the median redshift of the matched H-ATLAS-GAMA sample is below the median redshift for the full GAMA sample at the same M_r.

We see from the left-hand panel of Fig. 7 that in the lowest redshift range, $0 < z < 0.05$, the median colour versus magnitude relation does not depend on group mass over the whole mass range $10^{12} < M_{\mathrm{h}} < 10^{14}\,h^{-1}\,\mathrm{M}_{\odot}$, and is indistinguishable from the relation for all galaxies. The median far-IR-to-optical colour also depends only weakly on *r*-band absolute magnitude. The scatter around the colour–magnitude relation in groups also appears to be very similar to that for the field.

For the highest redshift range $0.1 < z < 0.2$, shown in the right-hand panel of Fig. 7, our estimated colour–magnitude relation and scatter lie just above the completeness boundary at all absolute magnitudes. We conclude from this that our measured colour–magnitude relation in this redshift range is probably determined mostly by the 250 μm flux limit of the H-ATLAS survey. Therefore, we cannot draw any firm conclusions about the real form of the colour–magnitude relation or its dependence on group mass at redshift $z > 0.1$ from these data. For the intermediate redshift range $0.05 < z < 0.1$, shown in the middle panel of Fig. 7, our median colour–magnitude relation falls on the selection boundary at faint magnitudes, and the lower 10-percentile value is close to the selection boundary even for brighter magnitudes. It therefore seems likely that the tilt in our estimated colour–magnitude relation in this redshift range is also mainly due to selection effects in the sample.

We further convert the 250 μm luminosity to SFR according to equation (3). The galaxy stellar mass is calculated using the $g-i$ colour and *i*-band luminosity, following the procedure in Taylor et al. (2011), and the SFR is calculated using individual temperatures for each source from SED fitting. We assume the Chabrier IMF for both the SFR and the stellar mass. The corresponding sSFR versus stellar mass relations at different redshifts are presented in Fig. 8. As in Fig. 7, it shows in the lowest redshift range, $0 < z < 0.05$, the median values of the sSFR as a function of galaxy stellar mass are indistinguishable between haloes of different masses, and the difference from those for all galaxies is very small. The scatter around the sSFR versus stellar mass relation is similar in groups of different mass, and also similar to those for the field. These results suggests that the sSFR versus stellar mass relation for dust-obscured star formation is almost independent of host halo mass for group masses $M_{\mathrm{h}} < 10^{14}\,h^{-1}\,\mathrm{M}_{\odot}$. Results for higher redshifts are limited

by the selection effect (grey region) as in Fig. 7 and thus no firm conclusions could be drawn from current data.

Our result is therefore that the far-IR/optical colour, and the sSFR for dust-obscured star formation, are independent of the group mass at a given optical luminosity or stellar mass. This is consistent with most previous work on the dependence of sSFR for star-forming galaxies on environment in the local Universe, using a variety of star formation tracers and measures of galaxy environment. Early studies using the Hα equivalent width (EW) as an indicator of sSFR found that this is independent of local galaxy density for the star-forming population, even though the fraction of galaxies classed as star-forming does change with environment (Balogh et al. 2004; Tanaka et al. 2004). Weinmann et al. (2006) used emission line SFRs to show that the sSFRs of actively star-forming galaxies at a given stellar mass depend only weakly on host halo mass over the range $10^{12} \lesssim M_{\rm h} \lesssim 10^{15}\,{\rm M}_{\odot}$, and Peng et al. (2010) found a weak dependence on local galaxy density using similar data. Bai et al. (2010) and McGee et al. (2011) used SFRs based on mid-IR and far-UV data respectively to show that the sSFRs of star-forming galaxies in groups were similar to those of field galaxies, although Bai et al. also found lower sSFRs in rich clusters. Indications of lower average SFRs for star-forming galaxies in clusters have also been found in some Hα studies (Gómez et al. 2003; Finn et al. 2005).

5 COMPARISON WITH GALAXY FORMATION MODEL PREDICTIONS

Semi-analytical modelling of galaxy formation in the ΛCDM framework has been proven very powerful in reproducing many observed properties of galaxies and their evolution (e.g. Cole et al. 2000; Baugh et al. 2005; Bower et al. 2006; Croton et al. 2006; De Lucia & Blaizot 2007; Guo et al. 2011b). However, until recently there has been only limited theoretical work combining galaxy formation models with modelling of the far-IR emission in a cosmological context (Granato et al. 2000; Devriendt & Guiderdoni 2000; Baugh et al. 2005; Lacey et al. 2008, 2010; Somerville et al. 2012). Here, we compare our measurements of the far-IR LF in groups to predictions from the GALFORM semi-analytical model (Cole et al. 2000). GALFORM incorporates a treatment both of the absorption of starlight by dust in galaxies and of the far-IR emission by the dust heated in this way (see Lacey et al. 2011 and Lacey et al., in preparation for more details). We show predictions from three different versions of the GALFORM model, namely Baugh et al. (2005), Bower et al. (2006), and Lacey et al., in preparation. These models differ in several ways. The Baugh et al. (2005) model has a top-heavy IMF for stars formed in starbursts, which was introduced in order to reproduce the number counts and redshift distribution of the faint sub-mm galaxy population detected at 850 μm. The Bower et al. (2006) model has a single IMF and includes active galactic nucleus (AGN) feedback, but does not reproduce the sub-mm galaxies. The Lacey et al., in preparation model includes both AGN feedback and a top-heavy IMF in starbursts (though less top heavy than that used in the Baugh et al. model). It matches the number counts and redshift distribution at 850 μm, and was also adjusted to approximately fit the observed number counts in the 250, 350, and 500 μm bands. None of these models had their parameters adjusted with reference to any observed properties of galaxy groups, so these are 'blind' predictions. Rather than identify galaxy groups in the GALFORM simulations in the same way as stop done for the GAMA group catalogue, we simply plot CLFs for virialized dark matter haloes of different masses.

The results are presented in Fig. 9. The red curves with errorbars are our observational results for groups with multiplicity $n \geq 2$. The dashed curves in different colours show the predictions for the three different GALFORM models. We first emphasize that all the models predict that the amplitude of the CLF (i.e. the number of galaxies per group) increases with group mass and with redshift, in qualitative agreement with our observational measurements. In general, the predictions from the Baugh et al. (2005) model are in best agreement with our measured far-IR CLFs, though this model still predicts too many galaxies with high far-IR luminosities in lower mass groups. The Bower et al. (2006) model underestimates the abundance of far-IR galaxies over the whole range of group mass and redshift studied here, generally by a large factor. The predictions of the Lacey et al., in preparation model lie between those of the other two models. None of the models reproduces the trend of characteristic far-IR luminosity strongly increasing with halo mass that we see in the observations. We conclude that the observations of the far-IR CLFs of groups can put stringent new constraints on galaxy formation models, which are complementary to the standard observational constraints (such as from galaxy LFs) that are typically used. In particular, the far-IR CLFs of groups tightly constrain how star formation in galaxies depends on the host halo mass, which in turn puts constraints on physical processes in galaxy formation models such as gas cooling, stripping and feedback from supernovae and AGN. We plan to explore these constraints in more detail in a future paper.

6 DISCUSSION AND CONCLUSIONS

Observations at far-IR wavelengths are an essential complement to the traditional UV and optical tracers of star formation. We have combined far-IR data from the H-ATLAS survey with the galaxy group catalogue from the GAMA optical spectroscopic survey to study the far-IR LFs of galaxies in different group environments and at different redshifts. We use a sample of 10.5 k galaxies from the H-ATLAS survey, flux limited at 250 μm with $S(250) > 32$ mJy, and matched to r-band selected galaxies with $r < 19.4$ in the GAMA spectroscopic survey, together with a catalogue of 10.7 k GAMA groups in the same region. We have used two independent methods to estimate the conditional far-IR LFs of groups. One is to directly identify the group membership of each far-IR source by matching to its optical counterpart. The other is to count the average excess number of far-IR galaxies within the optically estimated radius of each group. The measured far-IR LFs as a function of group mass and redshift are consistent between these two methods, but the results from the direct method are less noisy, so we use the direct method for most of our analysis. We find that the far-IR LFs are insensitive to the group optical multiplicity for a given group mass and redshift. We have measured average far-IR LFs in bins of mass and redshift over a range of $10^{12} < M_{\rm h} < 10^{14}\,h^{-1}\,{\rm M}_{\odot}$ in group mass and a range of $0 < z < 0.4$ in redshift, probing galaxy IR luminosities $L_{\rm IR} > 2 \times 10^{9}\,h^{-2}\,{\rm L}_{\odot}$.

We find that the far-IR LFs of groups are well fitted by a modified Schechter function, as previously found for the field population. We find that the characteristic far-IR luminosity L_* of galaxies in groups increases with the group mass below $10^{13}h^{-1}{\rm M}_{\odot}$, while at higher masses it flattens or turns over. The redshift dependence of L_* is a strong function of group mass. For very massive systems, L_* at $z \sim 0.3$ is 2.5 times larger than at $z \sim 0$, while this difference between high and low redshifts nearly vanishes for group masses below $10^{12.5}h^{-1}{\rm M}_{\odot}$. By integrating over the far-IR LF of galaxies in groups, we calculate the ratio $L_{\rm IR}/M_{\rm h}$ of total IR luminosity

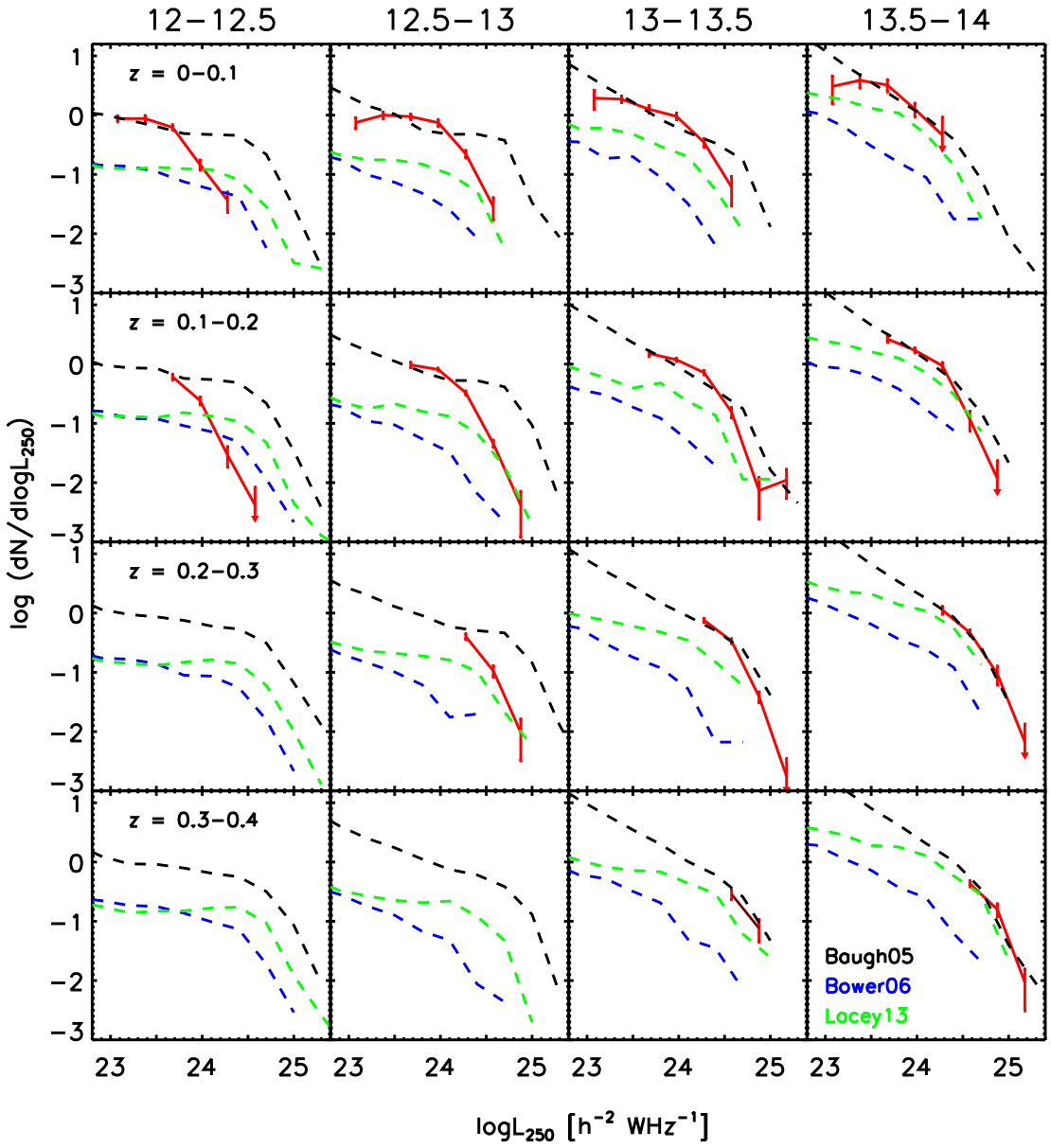

Figure 9. Comparison between the observational group CLFs and galaxy formation model predictions. Red solid curves show our measurements for H-ATLAS groups with optical multiplicity $n \geq 2$. Dashed curves show predictions for different GALFORM models, as indicated in the key.

to group mass. We find that this ratio is a decreasing function of group mass and an increasing function of redshift, being fit by $L_{\rm IR}/M_{\rm h} \propto M_{\rm h}^{-0.65}(1+z)^5$. We estimate that for $z < 0.2$, around 70 per cent of the total far-IR luminosity density is contributed by galaxies in haloes more massive than $10^{12}\,{\rm h}^{-1}\,{\rm M}_{\odot}$.

We also use our H-ATLAS/GAMA galaxy sample to measure the relation between far-IR/*r*-band colour and *r*-band absolute magnitude in the field and in groups of different mass. For $z < 0.05$, we find that for far-IR detected galaxies this relation is independent of group mass over the whole range $10^{12} < M_{\rm h} < 10^{14}\,h^{-1}\,{\rm M}_{\odot}$, and the same as that in the field. Similarly, we find the average-derived sSFR has only a weak dependence on galaxy stellar mass, and the sSFR versus stellar mass relation is indistinguishable in different environments. Again, this result applies to galaxies in our sample with detectable far-IR emission. This result is consistent with most previous studies of the dependence of SFRs of actively star-forming galaxies on environment using UV and optical tracers (e.g. Balogh et al. 2004; Tanaka et al. 2004; Weinmann et al. 2006; Peng et al. 2010; McGee et al. 2011). For $z > 0.05$, we find that no firm conclusions can be drawn about the far-IR/optical colour–magnitude relation from this sample, due to the far-IR flux limit.

We compared our results on the far-IR LFs of groups to three different semi-analytical galaxy formation models which have already proven successful in producing many other galaxy properties both at high and low redshifts. All these models qualitatively reproduced the trend of the characteristic far-IR luminosity L_* increasing with group mass and redshift. However, none of them were able to reproduce the observed conditional far-IR LFs in detail. This implies some deficiency in the way physical processes such as gas cooling, star formation and feedback are calculated in current galaxy formation models, but also demonstrates the potential for using such observations to distinguish between different models.

Our comparison with the models assumed that the galaxy groups identified in the GAMA survey correspond closely in both galaxy membership and total mass to the dark matter haloes in the theoretical galaxy formation models. In future work, we plan to test these assumptions by constructing mock galaxy catalogues from the models and applying the same algorithms for identifying groups and measuring their far-IR LFs as for the observations.

The analysis in this paper is based entirely on far-IR luminosities, which trace the dust-obscured component of galaxy SFRs, while the unobscured component of galaxy SFRs is traced by their far-UV luminosities. Most of the area covered by H-ATLAS Phase I and GAMA surveys also has far-UV imaging from *GALEX*. In a future paper, we plan to combine the far-IR and far-UV data from H-ATLAS and GAMA to estimate total galaxy SFRs free from biases due to dust obscuration, and use these to study their dependence on environment and redshift, in a similar way as done here for the far-IR luminosities.

ACKNOWLEDGEMENTS

The authors thank Michal Michalowski and Jochen Liske for useful comments. QG acknowledges support from a Newton International Fellowship, the NSFC grants (Nos 11143005 and No.11133003) and the Strategic Priority Research Program, The Emergence of Cosmological Structure of the Chinese Academy of Sciences (No. XDB09000000). PN acknowledges the support of the Royal Society through the award of a University Research Fellowship and the European Research Council, through receipt of a Starting Grant (DEGAS-259586). CSF acknowledges a Royal Society Wolfson Research Grant Award. This work was supported in part by the Science and Technology Facilities Council rolling grant ST/F001166/1 to the ICC. Calculations were partly performed on the ICC Cosmology Machine, which is part of the DiRAC Facility jointly funded by STFC and Durham University.

The H-ATLAS is a project with *Herschel*, which is an ESA space observatory with science instruments provided by European-led Principal Investigator consortia and with important participation from NASA. The H-ATLAS web site is http://www.h-atlas.org/.

GAMA is a joint European–Australian project based around a spectroscopic campaign using the Anglo-Australian Telescope. The GAMA input catalogue is based on data taken from the Sloan Digital Sky Survey and the UKIRT Infrared Deep Sky Survey. Complementary imaging of the GAMA regions is being obtained by a number of independent survey programme including GALEX MIS, VST KiDS, VISTA VIKING, WISE, H-ATLAS, GMRT, and ASKAP providing UV to radio coverage. GAMA is funded by the STFC (UK), the ARC (Australia), the AAO, and the participating institutions. The GAMA web site is http://www.gama-survey.org/.

The H-ATLAS and GAMA data will become public in the future. Details can be found on their websites. For more information about the model galaxy catalogues please contact the corresponding authors.

REFERENCES

Avni Y., Bahcall J. N., 1980, ApJ, 235, 694
Bai L., Rieke G. H., Rieke M. J., Hinz J. L., Kelly D. M., Blaylock M., 2006, ApJ, 639, 827
Bai L. et al., 2007, ApJ, 664, 181
Bai L., Rieke G. H., Rieke M. J., Christlein D., Zabludoff A. I., 2009, ApJ, 693, 1840
Bai L., Rasmussen J., Mulchaey J. S., Dariush A., Raychaudhury S., Ponman T. J., 2010, ApJ, 713, 637
Baldry I. K. et al., 2010, MNRAS, 404, 86
Balogh M. L., Couch W. J., Smail I., Bower R. G., Glazebrook K., 2002, MNRAS, 335, 10
Balogh M. et al., 2004, MNRAS, 348, 1355
Baugh C. M., Lacey C. G., Frenk C. S., Granato G. L., Silva L., Bressan A., Benson A. J., Cole S., 2005, MNRAS, 356, 1191
Berlind A. A., Weinberg D. H., 2002, ApJ, 575, 587
Biviano A., Fadda D., Durret F., Edwards L. O. V., Marleau F., 2011, A&A, 532, A77
Bower R. G., Benson A. J., Malbon R., Helly J. C., Frenk C. S., Baugh C. M., Cole S., Lacey C. G., 2006, MNRAS, 370, 645
Brinchmann J., Charlot S., White S. D. M., Tremonti C., Kauffmann G., Heckman T., Brinkmann J., 2004, MNRAS, 351, 1151
Buat V. et al., 2007, ApJS, 173, 404
Butcher H., Oemler A., Jr, 1978, ApJ, 219, 18
Chabrier G., 2003, PASP, 115, 763
Chung S. M., Gonzalez A. H., Clowe D., Markevitch M., Zaritsky D., 2010, ApJ, 725, 1536
Cole S., Lacey C. G., Baugh C. M., Frenk C. S., 2000, MNRAS, 319, 168
Croton D. J. et al., 2006, MNRAS, 365, 11
De Bernardis F., Cooray A., 2012, ApJ, 760, 14
De Lucia G., Blaizot J., 2007, MNRAS, 375, 2
Devriendt J. E. G., Guiderdoni B., 2000, A&A, 363, 851
Dressler A., 1980, ApJ, 236, 351
Driver S. P. et al., 2009, Astron. Geophy., 50, 050000
Driver S. P. et al., 2011, MNRAS, 413, 971
Dunne L., Eales S. A., 2001, MNRAS, 327, 697
Dunne L. et al., 2011, MNRAS, 417, 1510
Dye S. et al., 2010, A&A, 518, L10
Eales S. et al., 2010a, PASP, 122, 499
Eales S. A. et al., 2010b, A&A, 518, L23
Elbaz D. et al., 2007, A&A, 468, 33
Felten J. E., 1976, ApJ, 207, 700
Finn R. A., Zaritsky D., McCarthy D. W., Jr, 2004, ApJ, 604, 141
Finn R. A. et al., 2005, ApJ, 630, 206
Finn R. A. et al., 2010, ApJ, 720, 87
Gallego J., Zamorano J., Aragon-Salamanca A., Rego M., 1995, ApJ, 455, L1
Geach J. E. et al., 2006, ApJ, 649, 661
Giodini S. et al., 2012, A&A, 538, A104
Gómez P. L. et al., 2003, ApJ, 584, 210
Goto T. et al., 2010, A&A, 514, A7
Granato G. L., Lacey C. G., Silva L., Bressan A., Baugh C. M., Cole S., Frenk C. S., 2000, ApJ, 542, 710
Griffin M. J. et al., 2010, A&A, 518, L3
Guo Q., White S. D. M., 2008, MNRAS, 384, 2
Guo Q. et al., 2011a, MNRAS, 412, 2277
Guo Q. et al., 2011b, MNRAS, 413, 101
Han J. et al., 2014, preprint (arXiv:1404.6828)
Hauser M. G. et al., 1998, ApJ, 508, 25
Hill D. T. et al., 2011, MNRAS, 412, 765
Hopkins A. M., 2007, in Afonso J., Ferguson H. C., Mobasher B., Norris R., eds, ASP Conf. Ser. Vol. 380, Deepest Astronomical Surveys. Astron. Soc. Pac., San Francisco, p. 423
Ideue Y. et al., 2012, ApJ, 747, 42
Ilbert O. et al., 2009, ApJ, 690, 1236
Jing Y. P., Mo H. J., Boerner G., 1998, ApJ, 494, 1
Kelvin L. S. et al., 2012, MNRAS, 421, 1007
Kennicutt R. C., Jr, 1998, ARA&A, 36, 189
Kimm T. et al., 2009, MNRAS, 394, 1131
Kodama T., Balogh M. L., Smail I., Bower R. G., Nakata F., 2004, MNRAS, 354, 1103
Koyama Y. et al., 2008, MNRAS, 391, 1758
Koyama Y., Kodama T., Shimasaku K., Hayashi M., Okamura S., Tanaka I., Tokoku C., 2010, MNRAS, 403, 1611

Lacey C. G., Baugh C. M., Frenk C. S., Silva L., Granato G. L., Bressan A., 2008, MNRAS, 385, 1155
Lacey C. G., Baugh C. M., Frenk C. S., Benson A. J., Orsi A., Silva L., Granato G. L., Bressan A., 2010, MNRAS, 405, 2
Lacey C. G., Baugh C. M., Frenk C. S., Benson A. J., 2011, MNRAS, 412, 1828
Le Floc'h E. et al., 2005, ApJ, 632, 169
Lewis I. et al., 2002, MNRAS, 334, 673
Lilly S. J., Le Fevre O., Hammer F., Crampton D., 1996, ApJ, 460, L1
Loveday J. et al., 2012, MNRAS, 420, 1239
Madau P., della Valle M., Panagia N., 1998, MNRAS, 297, L17
McGee S. L., Balogh M. L., Wilman D. J., Bower R. G., Mulchaey J. S., Parker L. C., Oemler A., 2011, MNRAS, 413, 996
Merson A. I. et al., 2013, MNRAS, 429, 556
Metcalfe L., Fadda D., Biviano A., 2005, Space Sci. Rev., 119, 425
Oliver S. J. et al., 2010, A&A, 518, L21
Oliver S. J. et al., 2012, MNRAS, 424, 1614
Parry O. H., Eke V. R., Frenk C. S., 2009, MNRAS, 396, 1972
Peng Y.-j. et al., 2010, ApJ, 721, 193
Pilbratt G. L. et al., 2010, A&A, 518, L1
Poglitsch A. et al., 2010, A&A, 518, L2
Popesso P. et al., 2012, A&A, 537, A58
Puget J.-L., Abergel A., Bernard J.-P., Boulanger F., Burton W. B., Desert F.-X., Hartmann D., 1996, A&A, 308, L5
Reed D. S., Bower R., Frenk C. S., Jenkins A., Theuns T., 2007, MNRAS, 374, 2
Rigby E. E. et al., 2011, MNRAS, 415, 2336
Robotham A. S. G., Norberg P., Driver S. P., Baldry I. K., Bamford S. P., Hopkins A. M., Liske J. et al., 2011, MNRAS, 416, 2640
Roseboom I. G. et al., 2010, MNRAS, 409, 48
Roseboom I. G. et al., 2012, MNRAS, 419, 2758
Salim S. et al., 2007, ApJS, 173, 267
Saunders W., Rowan-Robinson M., Lawrence A., Efstathiou G., Kaiser N., Ellis R. S., Frenk C. S., 1990, MNRAS, 242, 318
Smith D. J. B. et al., 2011, MNRAS, 416, 857
Sobral D., Best P. N., Smail I., Geach J. E., Cirasuolo M., Garn T., Dalton G. B., 2011, MNRAS, 411, 675
Somerville R. S., Gilmore R. C., Primack J. R., Domínguez A., 2012, MNRAS, 423, 1992
Springel V. et al., 2005, Nature, 435, 629
Steidel C. C., Adelberger K. L., Giavalisco M., Dickinson M., Pettini M., 1999, ApJ, 519, 1
Sutherland W., Saunders W., 1992, MNRAS, 259, 413
Tanaka M., Goto T., Okamura S., Shimasaku K., Brinkmann J., 2004, AJ, 128, 2677
Taylor E. N. et al., 2011, MNRAS, 418, 1587
Tran K.-V. H., Saintonge A., Moustakas J., Bai L., Gonzalez A. H., Holden B. P., Zaritsky D., Kautsch S. J., 2009, ApJ, 705, 809
Webb T. et al., 2013, AJ, 146, 84
Weinmann S. M., van den Bosch F. C., Yang X., Mo H. J., 2006, MNRAS, 366, 2
Weinmann S. M., Kauffmann G., von der Linden A., De Lucia G., 2010, MNRAS, 406, 2249
Welikala N., Connolly A. J., Hopkins A. M., Scranton R., Conti A., 2008, ApJ, 677, 970
Yang X., Mo H. J., van den Bosch F. C., 2003, MNRAS, 339, 1057

APPENDIX A: GROUP CLFS WITH THE STACKING METHOD

In this appendix, we give a few more details about the stacking method and the results obtained using it.

Our stacking method for measuring the CLF in groups involves subtracting the estimated local background density of galaxies from the total projected counts, which means that our results might be affected by how we measure this background. We estimate the local background density within an annulus around each group. If we make the radius of this annulus too small, then our background estimate may include galaxies associated with the group due to clustering, causing us to overestimate the background and so underestimate the CLF of group members. On the other hand, if we make the annulus too large, we may fail to properly subtract the effect of foreground or background structures, again causing an error in the measured CLF. Here, we test the effect on the measured CLFs of varying the inner and outer radii of the annuli, where these are taken to be fixed multiples of the group radius R_{100}. The results are shown in Fig. A1, split by group mass and redshift, with radius range of the annulus in units of R_{100} for each coloured line shown by the key in the bottom-left panel. This figure shows that our measured CLFs are not very sensitive to the choice of annulus for the background subtraction.

In Fig. A2, we show the group CLFs measured using the stacking method (in black). These CLFs are noisier than those measured using the direct method (shown in Fig. 4). We also show the analytic fits using equation (6) to the measured CLFs from the stacking method (in red) and from the direct method (in blue). It can be seen that the fits from the stacking method agree reasonably well with those from the direct method in all group mass and redshift ranges.

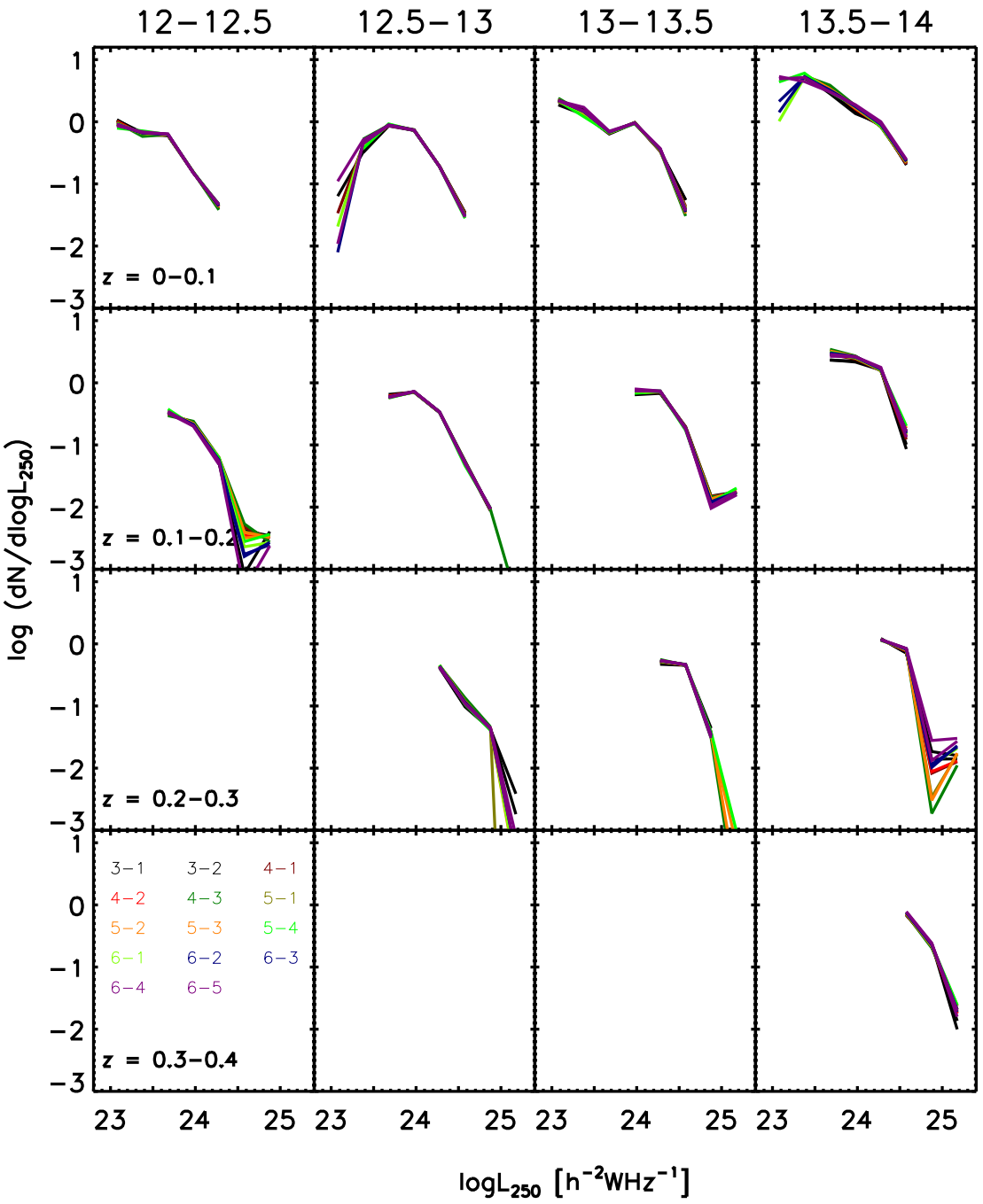

Figure A1. Conditional far-IR luminosity functions of galaxy groups measured with the stacking method for different choices of local background subtraction. The background number density around each group is estimated in an annulus. The different choices for the outer inner radii of these annuli in units of the group radius R_{100} are indicated in the bottom-left panel (see text for details.)

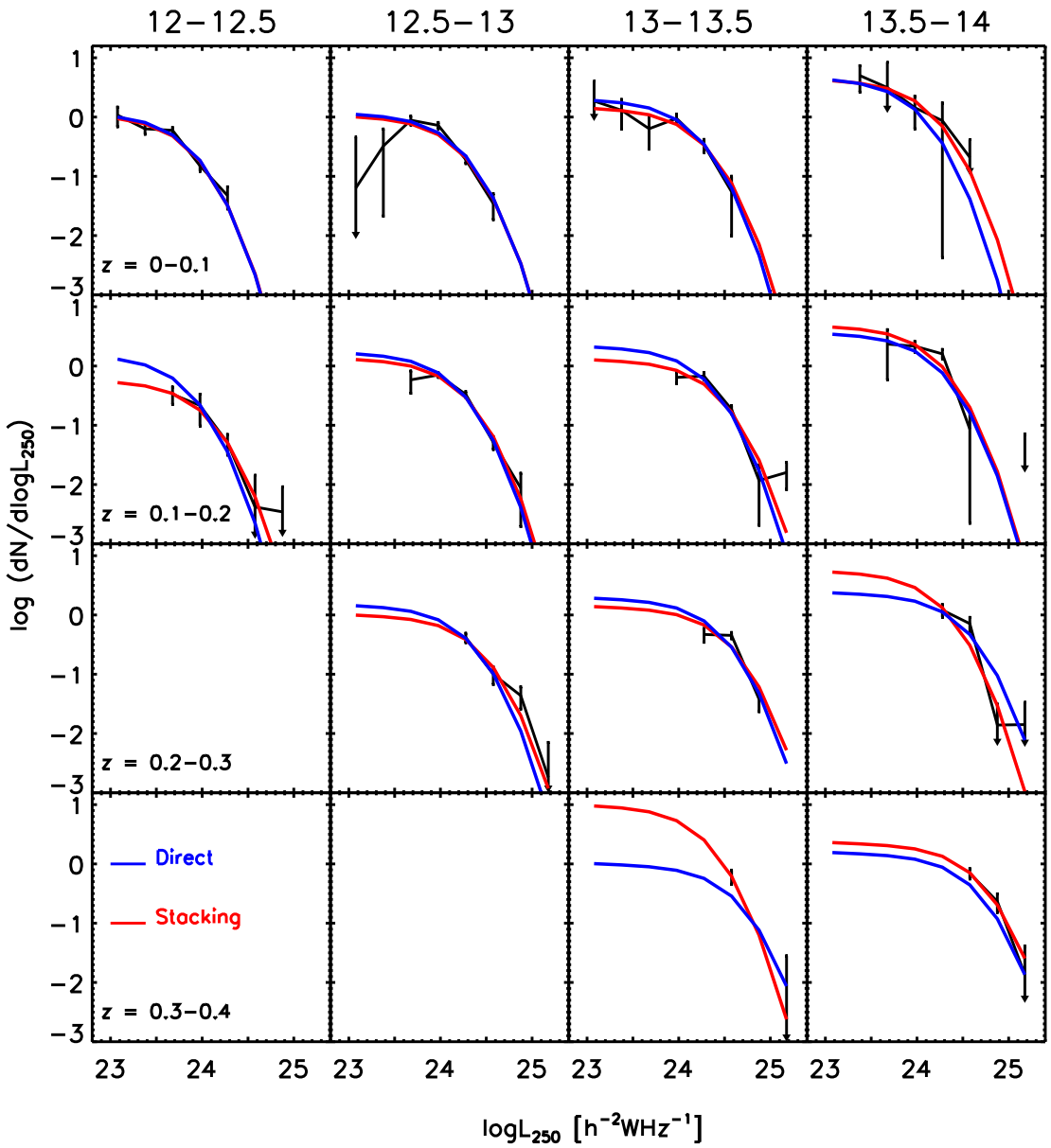

Figure A2. Conditional far-IR luminosity functions of galaxies in groups measured using the stacking method. The black lines with errorbars are the direct measurement, and the red curves are the analytic fits to these. The blue curves replicate the analytic fits from the direct method. Note that in most panels, the measurements are quite noisy, and these blue curves fits the stacking method measurements reasonably well. The parameters α and σ in equation (6) are fixed at 1.06 and 0.30, as measured from the field luminosity function. The redshift ranges are indicated in the first column and the group mass ranges are indicated on the top of each panel in the first row.

This paper has been typeset from a TEX/LATEX file prepared by the author.